

Geochemistry, Geophysics, Geosystems®



RESEARCH ARTICLE

10.1029/2021GC010198

Special Section:

Carbon degassing through volcanoes and active tectonic regions

Key Points:

- The total CO₂ output from Duvalo “volcano” has been estimated for the first time
- Gas compositions rule out significant mantle contributions or recent volcanic activity while geothermal activity is improbable
- An active fault system favors indirect gas production and upflow to the Earth's surface

Correspondence to:

W. D'Alessandro,
walter.dalessandro@ingv.it

Citation:

Li Vigni, L., Cardellini, C., Temovski, M., Ionescu, A., Molnár, K., Palcsu, L., et al. (2022). Duvalo “volcano” (North Macedonia): A purely tectonic-related CO₂ degassing system. *Geochemistry, Geophysics, Geosystems*, 23, e2021GC010198. <https://doi.org/10.1029/2021GC010198>

Received 6 OCT 2021

Accepted 20 JAN 2022

Duvalo “Volcano” (North Macedonia): A Purely Tectonic-Related CO₂ Degassing System

L. Li Vigni^{1,2} , C. Cardellini³ , M. Temovski⁴ , A. Ionescu^{3,4,5}, K. Molnár⁴ , L. Palcsu⁴, A. L. Gagliano², S. Cappuzzo², and W. D'Alessandro²

¹Dipartimento di Scienze della Terra e del Mare, Università di Palermo, Palermo, Italy, ²Istituto Nazionale di Geofisica e Vulcanologia (INGV) – Sezione di Palermo, Palermo, Italy, ³Dipartimento di Fisica e Geologia, Università di Perugia, Perugia, Italy, ⁴Isotope Climatology and Environmental Research Centre, Institute for Nuclear Research, Debrecen, Hungary, ⁵ISUMADECIP, Faculty of Environmental Science and Engineering, Babes-Bolyai University, Cluj-Napoca, Romania

Abstract Duvalo “volcano” is a site of anomalous geogenic degassing close to Ohrid (North Macedonia) not related to volcanic activity, despite its name. CO₂ flux measurements made with the accumulation chamber (321 sites over ~50,000 m²) showed fluxes up to nearly 60,000 g m⁻² d⁻¹, sustaining a total output of ~67 t d⁻¹. Soil gas samples were taken at 50 cm depth from sites with high CO₂ fluxes and analyzed for their chemical and isotope composition. The gas is mainly composed by CO₂ (>90%) with significant concentrations of H₂S (up to 0.55%) and CH₄ (up to 0.32%). The isotope compositions of He (R/R_A 0.10) and of CO₂ ($\delta^{13}\text{C}$ ~ 0‰) exclude significant mantle contribution, while $\delta^{13}\text{C}$ -CH₄ (~-35‰) and $\delta^2\text{H}$ -CH₄ (~-170‰) suggest a thermogenic origin for CH₄. The area is characterized by intense seismic activity and Duvalo corresponds to an active tectonic structure bordering the Ohrid graben. The production of H₂S within the stratigraphic sequence may be explained by thermochemical reduction of sulfate. The uprising H₂S is partially oxidized to sulfuric acid that, reacting with carbonate rocks, releases CO₂. The tectonic structure of the area favors fluid circulation, sustaining H₂S production and oxidation, CO₂ production and allowing the escape of the gases to the atmosphere. In the end, Duvalo represents a tectonic-related CO₂ degassing area whose gases originate mostly, if not exclusively, in the shallowest part of the crust (<10 km). This finding highlights that even systems with trivial mantle contribution may sustain intense CO₂ degassing (>1,000 t km⁻² d⁻¹).

Plain Language Summary The carbon cycle is an important piece of the puzzle of the present climate change. While anthropogenic sources of atmospheric carbon are reasonably constrained, geological sources are much less. Among the latter, carbon release to the atmosphere in seismically active areas, though known from decades, is less studied. Here we estimate the total emission of carbon dioxide from Duvalo, an area near Ohrid (North Macedonia). The obtained value (67 metric tons per day) is comparable with some active volcanic areas in the region. Although local inhabitants call this area Duvalo volcano, no recent volcanic activity is recognized here. The composition of the gas released by this system seems also to rule out geothermal activity or deep contributions from the Earth's mantle. This study shows that natural degassing systems with relatively shallow crustal sources (few kilometers), may sustain intense gas emissions from the soil.

1. Introduction

During the last decades, there has been great interest in the scientific community in estimating the degassing flux of carbon from the Earth's interior to the atmosphere. Among the greenhouse gases, carbon dioxide and methane are considered to be the most effective species contributing to the global warming. In 2011, the global abundance of CO₂ and CH₄ was, respectively, 391 ppm and 1,803 ppb (IPCC, 2014), but still increasing. The observations for 2018 reported in the fifteenth WMO Greenhouse Gas Bulletin show a global mean abundance of CO₂ and CH₄ respectively of 407.8 ± 0.1 ppm and 1,869 ± 2 ppb (WMO, 2019). They represent the main contributors to the total amount of geogenic carbon degassing to the atmosphere, playing a crucial role in the global carbon cycle (Delmelle & Stix, 1999). Despite a significant improvement in the worldwide data set, the global flux of CO₂ degassing from the Earth's interior is still the least well-quantified part of the global cycle (Berner & Lasaga, 1989). On geological time scales, the evolution of atmospheric CO₂ levels and Earth climate was mainly controlled by the competing effect of deeply derived CO₂ flux into the atmosphere and the atmospheric CO₂ sink by chemical weathering (Kerrick & Caldeira, 1993).

© 2022 The Authors.

This is an open access article under the terms of the [Creative Commons Attribution-NonCommercial License](#), which permits use, distribution and reproduction in any medium, provided the original work is properly cited and is not used for commercial purposes.

Many studies have been devoted to the quantification of the release of deeply derived CO₂ to the atmosphere from different geological settings (e.g., Brune et al., 2017; Kerrick, 2001; Mörner & Etiope, 2002) and most of them have focused on the present-day CO₂ emission from volcanoes (Brantley & Koepnick, 1995; Burton et al., 2013; Fischer & Aiuppa, 2020; Fischer et al., 2019; Le Guern, 1982; Werner et al., 2019). However, the close relationship between tectonically active areas and geogenic carbon emissions has long been evidenced (Barnes et al., 1978; Irwin & Barnes, 1980) and several authors have attempted to estimate non-volcanic degassing, which contributes a globally significant amount of geogenic CO₂ (Chiodini et al., 1999, 2000, 2011; Frondini et al., 2019; Kerrick et al., 1995; Lewicki & Brantley, 2000; Seward & Kerrick, 1996; Tamburello et al., 2018; Yuçe et al., 2017). According to Barnes et al. (1978) and Irwin and Barnes (1980), the main tectonic degassing areas are located along geodynamically active regions. Fault zones play an important role in CO₂ transfer by creating preferential pathways for gas-carrying fluid transport from the deep crust or the mantle to the Earth's surface (Faulkner et al., 2010; Hunt et al., 2017; Muirhead et al., 2016), escaping through the soil into the atmosphere as result of pressure decrease (King, 1986). At a global scale, the geographical distribution and the amount of deeply derived CO₂ are controlled by regional normal/transcurrent faulting (Tamburello et al., 2018) and continental rift lengths (Brune et al., 2017).

Carbon dioxide discharges and the main active fault systems are widespread in the Balkan Peninsula. However, the estimation of geogenic CO₂ release from this area is still poorly quantified, and a first regional quantification has been attempted only for Greece (Daskalopoulou et al., 2019).

The Duvalo area is located close to the village of Kosel, in the Ohrid region, in the south-western part of the Republic of North Macedonia (Figures 1a and 1b). The natural phenomenon of intense soil degassing (in Macedonian, Duvalo literally means a place where it blows; a blowhole), is responsible for intense soil alteration (Figure 1c), that has damaged vegetation over a large area (many thousands of m²), and the deposition of elemental sulfur and sulfate minerals. Between the sixteenth and nineteenth centuries, during the Ottoman Empire, Duvalo was mined for sulfur, producing about 1,700 kg a⁻¹ that was transported to the gunpowder magazines in Thessaloniki, now in Greece, and Istanbul in Turkey (Šerif, 2001). In 1979, the City Council of Ohrid Municipality declared the Duvalo site a natural rarity with unique features, falling under category III as a Monument of Nature (Markoski et al., 2019).

The Duvalo locality is considered to be a volcanic area by local people due to the “rotten eggs” smell, sulfur exhalations, strong soil degassing and “eruptions” from “craters,” which are considered a trace of extinct volcanic activity. The presence of “craters,” the biggest has a diameter of 50 cm and a depth of 30 cm (Figure 1d), considered a sign of “volcanic” activity, are instead remnants of the past mining activity. Although the phenomenon was marked as a volcanic solfatara in the local geological literature (e.g., Kotevski, 1987), no volcanic rocks or volcanic activity has been documented in the recent geologic history of the Kosel area (Dumurdzanov & Ivanovski, 1978; Markoski et al., 2019). To support the “volcanic” assumption, during dry periods stronger sulfur smell and whistling sound are present, whilst during wet periods bubbling is the dominant sound (Trojanović, 1925). Furthermore, the area was affected by an increase in its activity with a significant emission of dense smoke, in May 2014. This increase was interpreted as not related to volcanic activity but as the result of filling of the cracks by rainwater, which increased the gas pressure in the subsurface and generated the emission of water vapor mixed with other gases (Markoski et al., 2019). The characteristic alterations of the surface are due to the reactions between the exhalations of H₂S and the oxygen dissolved in rainwater, forming sulfuric acid which alters the phyllite rocks, leading to their kaolinitization (Markoski et al., 2019). According to Hoffmann et al. (2010), the phenomenon is related to an active fault system present in the area.

Little research concerning the geochemical characterization of the gas manifestation of the area has been conducted (Trojanović, 1925; Iloski et al., 1957, as cited by Dumurdzanov & Ivanovski, 1978; Markoski et al., 2019). The gases consist of CO₂ (98%), H₂S (0.8%) and inert gases (1%), with a flux rate of 0.2 l s⁻¹. Between 1956 and 1957, in order to ascertain the sulfur reserves of the Duvalo area, the Office for Geological Research – Ohrid drilled two boreholes. An explosion occurred near one of the two boreholes and the analysis of the emitted gases were carried out, showing an increase of H₂S, up to 2% (Iloski et al., 1957, as cited by Markoski et al., 2019).

With the aim to better characterize the source of the Duvalo gas manifestation, the present study reports on new chemical and, for the first time, isotope data of the gas emissions. Furthermore, we present the first map of CO₂ soil diffuse degassing and estimate of the total CO₂ output for the area.

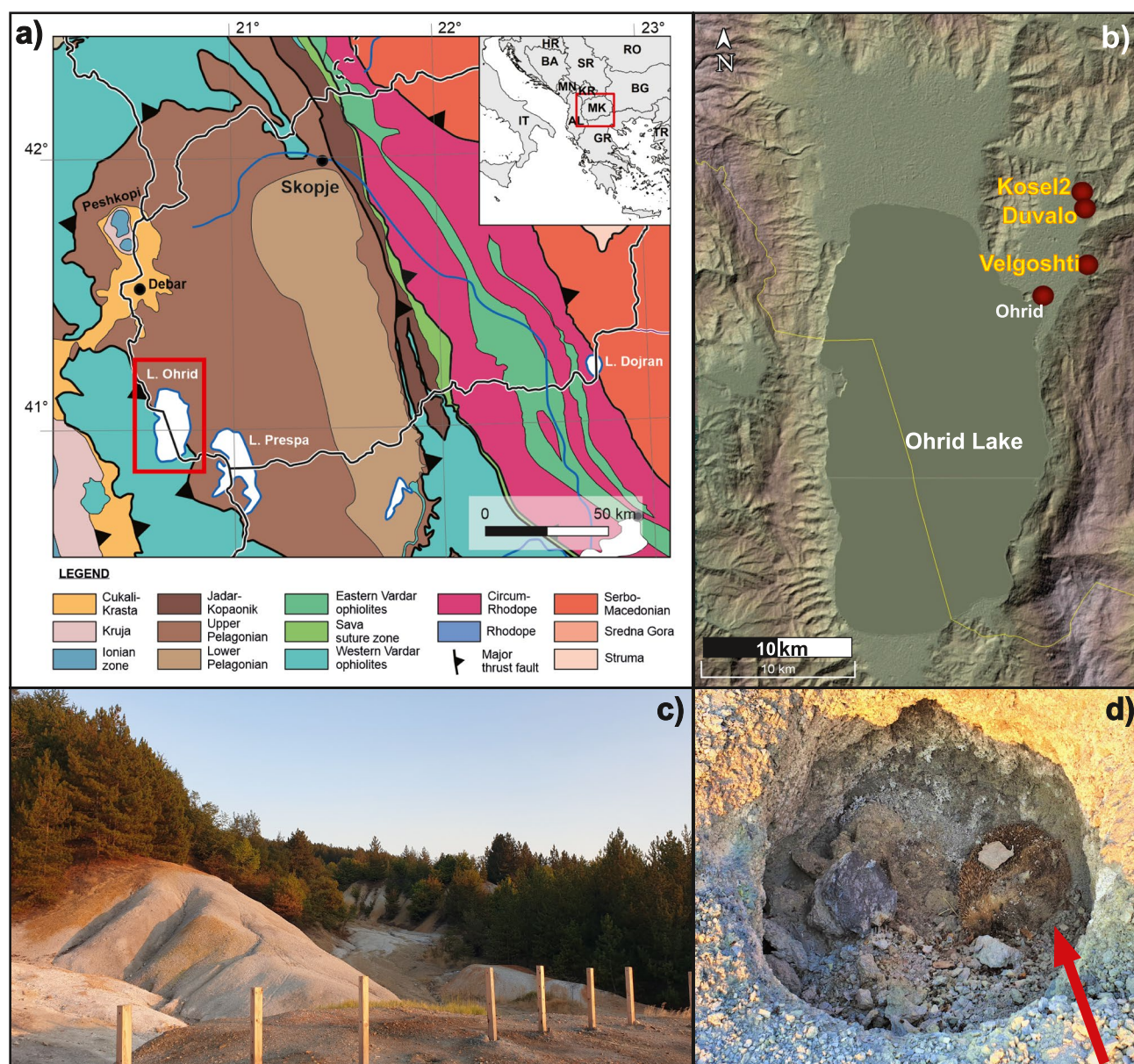


Figure 1. Location of the study area. (a) Ohrid region in relation to major geotectonic units of Republic of North Macedonia, adapted from Schmid et al. (2020); (b) elevation map of Ohrid Basin with geographic setting of Duvalo and Velogoshti sites; political border with Albania is shown in yellow line; (c) panoramic photo of Duvalo area; and (d) dead hedgehog (red arrow) inside a hole with strong gas exhalation.

2. Geological Setting

The Duvalo site, near Kosel village, is located in the north-eastern part of the Ohrid Basin, that hosts one of the oldest lakes in Europe, Lake Ohrid (Wagner et al., 2008). The Ohrid Basin is a graben structure, part of the Cenozoic South-Balkan Extensional Regime (Burchfiel et al., 2008; Dumurdzanov et al., 2005), that is flanked by active N-S striking normal faults, controlled by E-W extension since Pliocene (Dumurdzanov et al., 2005; Hoffmann et al., 2010), after initial opening as a pull-apart basin in Late Miocene (Lindhorst et al., 2015).

The Ohrid Basin is situated along the contact of two major tectonic units: the Mirdita Ophiolite Zone in the west, and the Western Macedonian Zone (also Korab Zone or West Pelagonian Zone) to the east (Dumurdzanov et al., 2005; Robertson & Shallo, 2000). A recent review by Schmid et al. (2020), places the Mirdita Zone within the Western Vardar ophiolitic units, obducted in Late Jurassic-Early Cretaceous onto the Adriatic margin, with

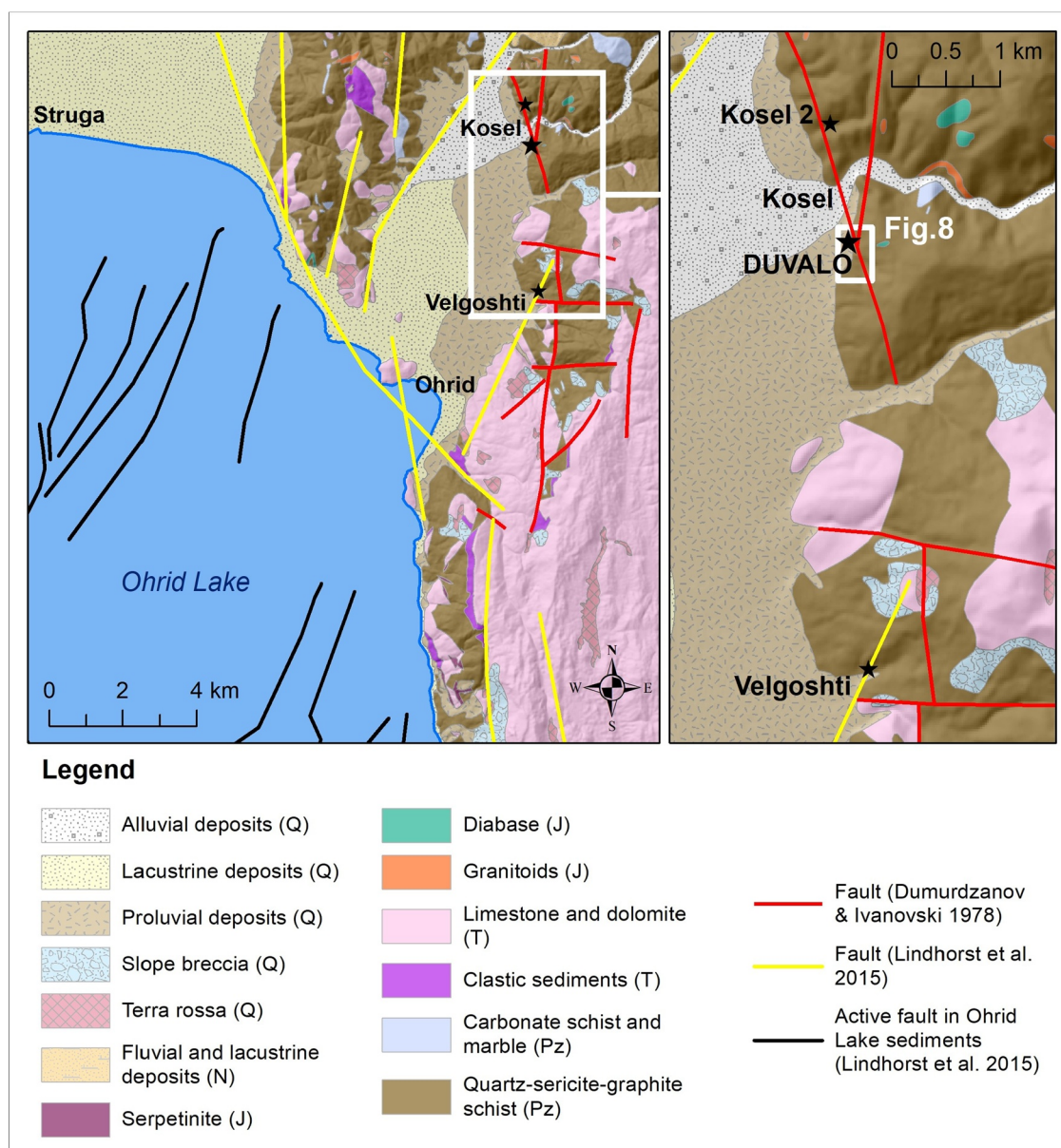


Figure 2. Geological settings of Duvalo site. Map compiled from geological data of Dumurdzanov and Ivanovski (1978) and Lindhorst et al. (2015). The geographical position of the sampling sites is evidenced by a star. The area investigated for CO₂ fluxes and mapped in Figure 8 is evidenced by a box in the map on the right.

the Korab Zone considered as part of the Upper Pelagonian unit, itself considered as an Adria-derived unit (Figure 1). The Upper Pelagonian is built of Paleozoic metamorphic rocks (various schists classified as a phyllite formation), which are superimposed by Triassic rocks that comprise a clastic-carbonate formation with diabase intrusions and rhyolite lava flows, and a cherty-carbonate formation composed of limestone and dolomite (Dumurdzanov & Ivanovski, 1978).

In the area around Kosel village, rocks of the phyllite formation mostly outcrop, composed of quartz-sericite schist, with lenses of quartz-sericite-graphitic schists, with also small intrusions of granitoids and diabase. To the southeast, Triassic marble tops Galichica Mountain. Duvalo is situated within the quartz-sericite schists, along an intersection of NNW and NNE striking faults (Figure 2). The latter follows the direction of an active fault within the sediments of Ohrid Lake (Lindhorst et al., 2015). The area is seismically active (Arsovsky & Hadžievsky, 1970; Dumurdzanov et al., 2016), with the most recent significant earthquake, with a magnitude of $M_L = 4.9$, registered nearby in 2017 (Bojadjieva et al., 2019). Strongly influenced by the nearby regions (Albania

and Northern Greece), the area of Ohrid is associated with one of the highest levels of seismic hazard (higher activity rate and maximum magnitude) in the country (Lee & Trifunac, 2017). The highest seismic activity occurs in the southern parts of the Ohrid graben, with notable earthquakes registered in 1906 ($M_w = 6.04$), 1911 ($M_w = 6.68$), and 1912 ($M_w = 6.04$), having epicenters in Ohrid Lake (Dumurdzanov et al., 2016). Hypocenters are shallow with depths between 10 and 25 km, although some earthquakes with depths between 25 and 50 km have been registered in close by areas (Hoffmann et al., 2010). Based on these sparse data, it is inferred that some of the active faults may reach the brittle-ductile transition zone at ~ 12 –25 km depth (Reicherter et al., 2011).

The gas exhalation area at Duvalo is easily recognized by the large zone devoid of vegetation and covered by light colored alteration products, bordered by a dense forest area. The trees at the limit of the exhaling area show chlorotic or necrotic leaves or needles especially on their lower branches. The area is elongated in NNW-SSE direction on the hillside bordering the Ohrid Plain and comprises also some minor areas separated by forest. At about one km north of Duvalo, along the NNW-striking fault, another area devoid of vegetation can be recognized (Kosel 2). Here only a few alteration areas may be found, with quartz-sericite-graphitic schists also exposed, while most of the area is extensively eroded and shows a very steep relief because of the highly erodible rocks. Similarly, the exposed parts of the quartz-sericite-graphitic schists can be found at about 4 km south of Duvalo, at the north-eastern outskirt of Velgoshti village, on a hill (thousands of m^2) covered by sparse stunted vegetation. Here, sulfur and sulfate efflorescence's and incrustations can be recognized along a 50 m stretch at the southern foot of the hill.

3. Materials and Methods

In August 2019 and March 2020, two sampling campaigns were carried out. Nine gas samples were collected in the study area: seven samples have been collected in the Duvalo area and one sample in each of the other two sites with evident alteration signs, Kosel 2 and Velgoshti (Figure 2). Samples were collected through a probe inserted in the soil at 50 cm depth and stored in glass vessels with two vacuum stopcocks and Exetainer© Labco vials (12 ml of volume). The chemical and isotope analyses were carried out at the laboratories of Istituto Nazionale di Geofisica e Vulcanologia of Palermo (INGV-Palermo).

The concentrations of He, H_2 , H_2S , O_2 , N_2 , CO_2 , CH_4 , and C_2H_6 in the samples were determined using an Agilent 7890B gas chromatograph with Ar as carrier, equipped with a 4-m Carbosieve S II and PoraPlot-U columns. A TCD detector was used to measure the concentrations of He, O_2 , N_2 , and CO_2 and a FID detector for CH_4 , and C_2H_6 . The analytical errors were estimated as less than 5% for He, H_2 , H_2S , and C_2H_6 and 3% for O_2 , N_2 , CH_4 , and CO_2 . Argon was analyzed using a Perkin Elmer XL gas-chromatograph with a MSieve 5A column, with the TCD detector having He as carrier.

An evacuated glass vessel filled with a 4M soda solution, which blocked CO_2 and H_2S as dissolved ions, was used to concentrate the minor gases in order to obtain the CH_4/C_2H_6 ratio of Duvalo sample in March 2020.

The $^{13}C/^{12}C$ ratios of CO_2 (expressed as $\delta^{13}C-CO_2$ ‰ vs. V-PDB) were measured using a Finnigan Delta S mass spectrometer after purification of the gas mixture by standard procedures using cryogenic traps (precision ± 0.1 ‰). Carbon and hydrogen isotopes of CH_4 were measured using a Thermo TRACE GC interfaced with a Delta Plus XP gas source mass spectrometer, equipped with a Thermo GC/C III (for carbon) and with GC/TC peripherals (for hydrogen). The $^{13}C/^{12}C$ ratios are reported as $\delta^{13}C-CH_4$ values (precision ± 0.2 ‰) with respect to the V-PDB standard while $^2H/^1H$ ratios are reported here as δ^2H-CH_4 values (precision ± 2.0 ‰) with respect to the V-SMOW standard. The abundance and isotope composition of He, and $^4He/^{20}Ne$ ratios, were determined by separately admitting He and Ne into a split flight tube mass spectrometer (Helix SFT). Helium isotope compositions are given as R/R_A , where R is the ($^3He/^4He$) ratio of the sample and R_A is the atmospheric ($^3He/^4He$) ratio ($R_A = 1.386 \times 10^{-6}$). The analytical errors were generally $< 1\%$.

The carbon dioxide flux was measured using the accumulation chamber method (Chiodini et al., 1998) at 321 sites with a portable soil fluxmeter (WEST Systems, Italy). Flux values were determined at each site from the rate of CO_2 concentration increase in the chamber and are expressed as grams per square meter per day ($g\ m^{-2}\ d^{-1}$) after conversion from volumetric to mass concentrations considering the measured atmospheric pressure and temperature values. The portable soil fluxmeter is equipped with a Licor LI820 IR spectrometer characterized by a reproducibility better than 20% in the measuring range 10–20,000 ppm. The used accumulation chamber has an

area of 0.031 m² and a volume of 0.0028 m³. Care was taken to follow the recommendations regarding instrument calibration, flux measurements and data elaboration as proposed by Lewicki et al. (2005). The entire data set is reported in Table A1 (Appendix A; Li Vigni et al., 2022a).

The CO₂ flux data were derived using statistical and geostatistical tools. To characterize the CO₂ flux the GSA method (Chiodini et al., 1998), based on Sinclair's partitioning method (Sinclair, 1974), was used. This method allows the partitioning of a polymodal statistical distribution into individual populations and the definition of the populations' statistical parameters and relative proportions. Because the gas flux data resulted a combination of log-normal distributed populations, the computed mean and standard deviation of the partitioned populations refer to the logarithm of CO₂ flux values. The mean of the CO₂ flux and the 95% confidence interval of the mean were thus estimated by the Sichel's t-estimator (David, 1977).

A map of the CO₂ fluxes was drawn using the sequential Gaussian simulations (sGs method; Cardellini et al., 2003). The sGs method consists of the production of numerous equiprobable realizations of the spatial distribution of the CO₂ flux using the *sgsim* algorithm of the *GSLIB* software library (Deutsch & Journel, 1998) according to the variogram model of the normal score of the CO₂ flux derived from the experimental variogram. One hundred equiprobable realizations were computed for the area using a computational grid of 2 × 2 m. The CO₂ flux map is then reported as map of the "expected" values at any cell (E-type estimates), obtained through a pointwise linear average of all the realizations (Deutsch & Journel, 1998). The results of the sGs were also used to estimate the total CO₂ output, summing the products of simulated value at each grid cell by the cell surface. The mean and the standard deviation of the 100 simulated values of total CO₂ output, computed for the 100 realizations, were assumed to be the characteristic values of the CO₂ output of its uncertainty for the area.

The soil temperature was measured at 50 cm depth by means of a digital thermocouple (error ±0.3°C in the range from −100°C to 200°C) only at five sites in August 2019.

4. Results

The chemical and isotope composition and geographic coordinates of the gas samples are reported in Table 1 (Li Vigni et al., 2022b). Generally, carbon dioxide, in four samples, and nitrogen and oxygen, in three samples, are the dominant components of the gas samples from the Duvalo area (Figure 3). Carbon dioxide arrives up to 966,100 μmol mol^{−1}, N₂ ranges from 17,900 to 736,100 μmol mol^{−1}, and O₂ concentrations vary between 128 and 189,700 μmol mol^{−1}, indicating sometimes an important air component. The gases collected at Kosel 2 and Velgoshti are dominated by the atmospheric component (N₂ and O₂), while CO₂ concentrations range from 2,900 to 8,700 μmol mol^{−1}, respectively. For all samples, hydrogen sulfide concentrations show a wide spectrum of values between <10 and 5,500 μmol mol^{−1}. Methane concentrations display also a large range, that varies between 11 and 3,250 μmol mol^{−1}. Minor compounds, hydrogen and helium, are also found, with concentrations of <3–1,010 μmol mol^{−1} for the former and <3–70 μmol mol^{−1} for the latter. Ethane is always below the detection limit (<10 μmol mol^{−1}) but the CH₄/C₂H₆ ratio (513) was measured in one sample in the enriched headspace gas of a soda ampule. Argon was measured only in few samples and showed absolute values and N₂/Ar ratios close to the atmospheric values in the samples of Kosel 2 and Velgoshti. On the contrary, Duvalo samples showed very low concentrations of argon (61 and 79 μmol mol^{−1}) and N₂/Ar ratios (>200) higher than atmospheric values.

The δ¹³C_{CO₂} at Duvalo ranges from −0.2‰ to 2.7‰ versus V-PDB, whilst Kosel 2 and Velgoshti have values of −13.7‰ and −0.8‰, respectively. The isotope composition of He was determined only in two samples from Duvalo, both having the value of 0.10 R/R_A. The isotope composition of CH₄ has also been determined showing δ¹³C_{CH₄} values that range from −36.8‰ to −34.4‰ V-PDB and δ²H_{CH₄} values that vary between −180‰ and −158‰ versus V-SMOW.

Soil CO₂ fluxes measured in the Duvalo area range from 1.34 to 59,300 g m^{−2} d^{−1} and were modeled as the combination of three log-normal populations (Figure 4), for which statistical parameters are reported in Table 2.

The populations B and C are characterized by elevated mean CO₂ flux values and may be considered to represent deep CO₂ degassing. The occurrence of two populations for the deep CO₂ degassing could reflect the relative prevalence of diffusive or advective CO₂ transport mechanisms (e.g., Chiodini et al., 2020). On the contrary, population A is characterized by a relatively low mean CO₂ flux and may represent the biological CO₂ background flux for the area. The mean CO₂ flux of population A (45 g m^{−2} d^{−1}) is actually slightly higher than the CO₂ fluxes

Table 1
Chemical and Isotopic Composition of the Gases

Name	Date	N (DD)	E (DD)	He (μmol/mol)	H ₂ (μmol/mol)	O ₂ (μmol/mol)	N ₂ (μmol/mol)	CH ₄ (μmol/mol)	CO ₂ (μmol/mol)
Duvalo	22.08.2019	41.16934	20.83719	70	38	128	17,900	3,250	966,100
Duvalo 2	24.08.2019	41.16705	20.83868	29	1,010	89,000	381,400	1,370	508,400
Duvalo 3	24.08.2019	41.16721	20.83924	<3	108	161,000	613,300	463	213,300
Duvalo 4	24.08.2019	41.16791	20.83914	<3	756	189,700	736,100	11	63,700
Duvalo	02.03.2020	41.16932	20.83721	62	<3	19,300	89,800	2870	882,600
Duvalo A	02.03.2020	41.16699	20.83865	56	<3	26,600	117,900	2740	850,800
Duvalo B	02.03.2020	41.16717	20.83918	51	<3	19,000	88,800	3,190	888,400
Kosel 2	02.03.2020	41.17961	20.83500	5	10	205,700	768,200	3.7	2900
Velgoshti	02.03.2020	41.13395	20.83919	5	31	137,800	841,800	31	8,700

Name	H ₂ S (μmol/mol)	C ₂ H ₆ (μmol/mol)	Ar (μmol/mol)	δ ¹³ C(CO ₂) ‰ (vs. V-PDB)	δ ¹³ C(CH ₄) ‰ (vs. V-PDB)	δ ² H(CH ₄) ‰ (vs. VSMOW)	R/R _A	Error	He/Ne
Duvalo	5,500	<10	79	−0.2	−34.4	−166	0.10	0.003	472
Duvalo 2	11	<10	n.a.	−0.1	−36.8	−158	n.a.	n.a.	n.a.
Duvalo 3	<10	<10	n.a.	2.7	n.a.	n.a.	n.a.	n.a.	n.a.
Duvalo 4	<10	<10	n.a.	−0.1	n.a.	n.a.	n.a.	n.a.	n.a.
Duvalo	5,200	5.6	61	−0.8	−34.5	−180	0.10	0.004	2066
Duvalo A	3,800	<10	n.a.	−0.8	−35.0	−175	n.a.	n.a.	n.a.
Duvalo B	4,300	<10	n.a.	−0.8	−36.5	−169	n.a.	n.a.	n.a.
Kosel 2	<10	<10	9,400	−13.7	n.a.	n.a.	n.a.	n.a.	n.a.
Velgoshti	<10	<10	10,000	−0.8	n.a.	n.a.	n.a.	n.a.	n.a.

Note. DD = decimal degrees; n.a. = not analyzed.

produced by the biological activity for different ecosystems presented in other studies (mean CO₂ flux from 0.2 to 21 g m^{−2} d^{−1}, Cardellini et al., 2017; Viveiros et al., 2010 and reference therein) and relatively high with respect to the biological background generally found in numerous hydrothermal sites (Chiodini et al., 2008 and references therein). However, a relatively high biological background CO₂ flux has also been reported for several sites; for example, mean background CO₂ fluxes of 44.8 and 46.85 g m^{−2} d^{−1} were reported at the Furnas do Enxofre degassing area (Azores; Viveiros et al., 2020) and at Horseshoe Lake (Mammoth Mountain, CA, Cardellini et al., 2003) respectively.

Temperatures were in the range of 17.2°C–18.5°C, higher than the mean annual atmospheric temperature of the area (11.1°C; Zikov, 1997), but close to the mean summer atmospheric temperature (19.7°C; Zikov, 1997) and lower than the atmospheric temperatures during the measurement campaign (from about 20°C in the early morning up to about 40°C in the afternoon).

Only two soil CO₂ flux measurements were made at Kosel 2 in areas with some signs of soil alteration, and in both cases low CO₂ flux values were measured (4.61 and 5.23 g m^{−2} d^{−1}). No flux measurement was made at the Velgoshti site.

5. Discussion

5.1. Origin of the Gases

The most CO₂-rich samples are consistent with previous analyses in 1925 (Trojanović, 1925), 1957 (Iloski et al., 1957; as reported in Markoski et al., 2019) and in 1977 (in Markoski et al., 2019), when it was reported that

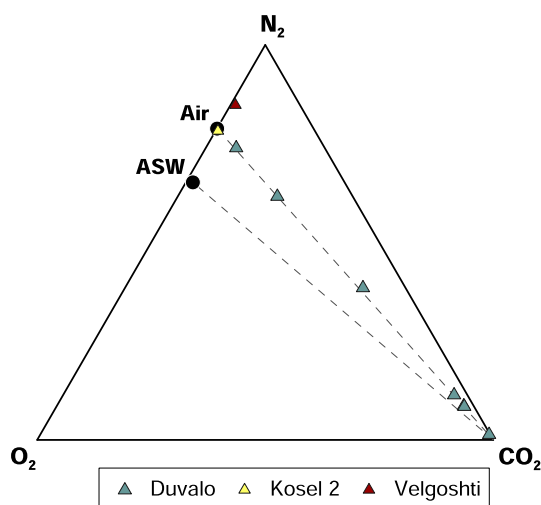


Figure 3. CO₂-N₂-O₂ ternary plot. The atmospheric air and air saturated water compositions are also plotted.

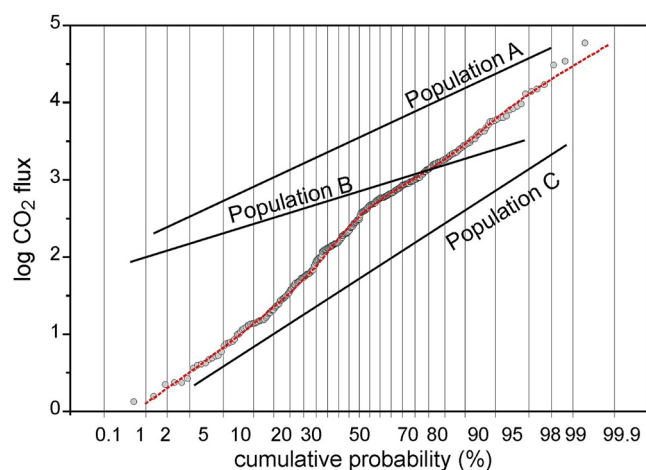


Figure 4. Probability plot of the CO₂ fluxes from Duvalo area. The black lines represent the partitioned populations while the dashed red line represent the combination of the partitioned populations according to their relative proportions (see Table 2).

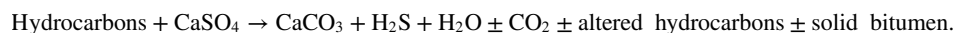
the gases were composed mainly of CO₂ (90%–98%) and H₂S (0.8%). The consistency of the results indicates a certain stability of the exhaling system, at least in the last century.

Here, isotope analyses were carried out to deduce the origin of the gas manifestations in the Duvalo area. Helium compositions have a R/R_A ratio of 0.1, which indicates an almost pure crustal origin (Figure 5a). Deep normal or transcurrent faults may act as a preferential pathway for upwelling of mantle helium, which may be recognized in R/R_A values tending toward MORB values ($8 \pm 1 R/R_A$; Ozima & Podosek, 2002). The Ohrid area is a seismically active extensional basin and the site of Duvalo corresponds to an active fault system. Such extensional basins are widespread in the neighboring areas. For the other tectonically similar areas in the south and in the north-west of the country, mantle contributions up to 20% (R/R_A up to 1.64) have been measured (Figure 5a; Temovski et al., 2020). Similarly high R/R_A values (up to 1.27) have been found also in northern Greece (Figure 5a; Daskalopoulou et al., 2018). On the contrary, at Duvalo a mantle contribution seems absent or at least trivial (about 1%). Similarly, $\delta^{13}\text{C}$ -CO₂ values between -0.8‰ and -0.1‰ and CO₂/He ratios between 7.6×10^{10} and 8.4×10^{10} point toward an almost pure crustal (marine limestones) source also for CO₂, with at most 2% mantle contribution (Figure 5b).

Data have been plotted in $\delta^{13}\text{C}$ -CH₄ versus $\delta^2\text{D}$ -CH₄ (Schoell, 1983) and CH₄/(C₂ + C₃) versus $\delta^{13}\text{C}$ -CH₄ (Bernard et al., 1977) space, modified by Milkov and Etiope (2018) in order to discriminate the origin of methane (Figure 6). The Duvalo samples fall within the thermogenic range, although secondary microbial or oxidation processes cannot be excluded (Milkov & Etiope, 2018 and reference therein).

The origin of H₂S in the gases released at Duvalo is somewhat harder to constrain. Unfortunately, no sulfur isotope data are available at present. H₂S is a typical gas of hydrothermal origin but in the present case we have no indication about the presence of a hydrothermal system at depth. No thermal springs are present at Duvalo or in the surrounding area. The closest thermal springs are more than 40 km away to NW. No thermal anomaly has been recognized within the soils of Duvalo and at 50 cm depth, even at the sites with the highest measured CO₂ fluxes, the soil temperatures were close to the mean atmospheric temperature of the area. The absence of thermal anomalies and the low temperature of the gases is not in itself an indication of absence of any geothermal system at depth. Nevertheless, the south-western part of Macedonia, to which the area belongs, is not considered to have anomalous heat flow (Popovska-Vasilevska & Armenski, 2016).

An alternative process that might produce H₂S is sulfate reduction (Machel, 2001), either microbially (MSR) or thermochemically (TSR). In both cases, the process can be schematized by the following reaction:



MSR is considered to occur at temperatures below 80°C while TSR generally in the 100°C–140°C range (Machel, 2001). TSR is thermodynamically favored, but kinetically limited, also at temperatures down to 25°C (Mougin et al., 2007).

In the study area, no hydrocarbon, gypsum or anhydrite deposits have been identified, either outcropping or in the subsoil. Nevertheless, organic-rich schists are present in the metamorphic basement part of the Upper Pelagonian in the area (Dumurdzanov & Ivanovski, 1978). Shists may be the origin of some hydrocarbons, and the CH₄ found in the gases released at Duvalo. The isotopic composition of the CH₄ suggests a thermogenic origin compatible with TSR processes (Milkov & Etiope, 2018). Despite their absence at the surface in the area of Duvalo, gypsum or anhydrite deposits may be present at depth. As suggested by Fraseri et al. (1996), the Peshkopi tectonic window in Albania to the north, which is part of the Ionian zone and underlies the Upper Pelagonian (Figure 1; Robertson & Shallo, 2000; Schmid

Table 2
Statistical Parameters of CO₂ Flux Populations

Populations	Mean log CO ₂ flux	σ log CO ₂ flux	Proportion (%)	Mean CO ₂ flux (g m ⁻² d ⁻¹)	95% confidence interval (g m ⁻² d ⁻¹)
A	1.32	0.54	30	45	35–62
B	2.71	0.46	59	897	746–1,128
C	3.65	0.50	11	8,382	6,289–15,161

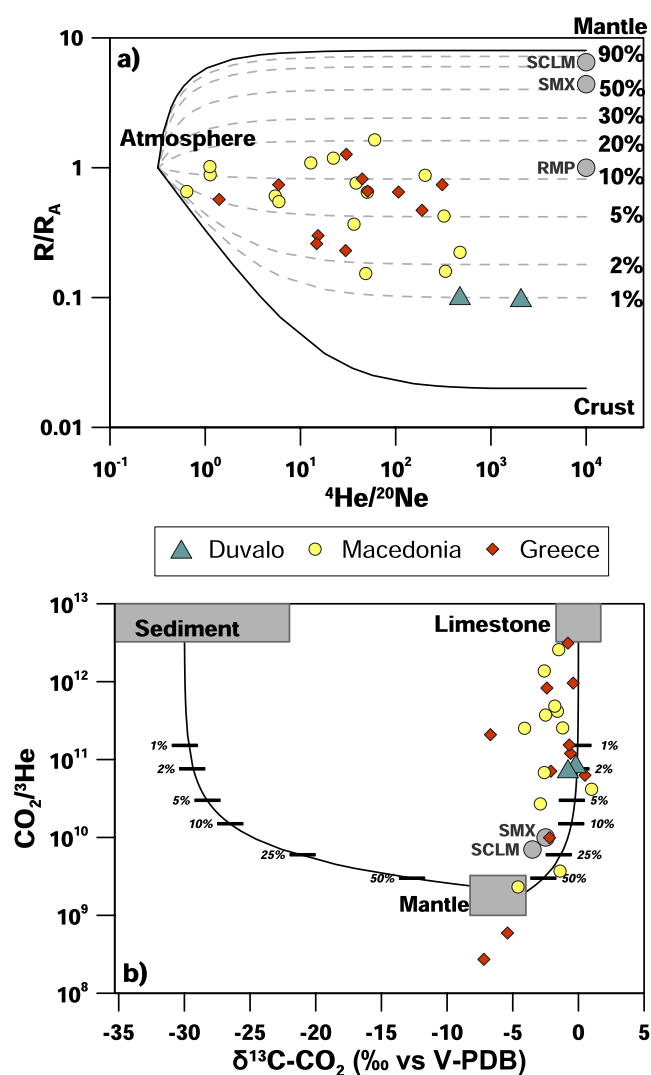


Figure 5. Binary plots of (a) R/R_A versus $^4\text{He}/^{20}\text{Ne}$ of the samples collected at Duvalo. The mixing lines between Atmosphere and a MORB-type Mantle and between Atmosphere and Crust are also plotted. Dashed lines represent mixing between atmosphere and end-members with different percentages of MORB-type mantle contribution (after Sano & Wakita, 1985). Three other mantle end-members are also reported: SCLM (Subcrustal Lithospheric Mantle – Gautheron & Moreira, 2002); SMX (Stromboli Mantle Xenoliths – Martelli et al., 2014); RMP (Roman Magmatic Province – Martelli et al., 2004); and (b) $\text{CO}_2/^3\text{He}$ versus $\delta^{13}\text{C}-\text{CO}_2$. The compositions for Sediments, MORB-like Mantle and Limestones end-members are: $\delta^{13}\text{C}-\text{CO}_2 = -30\text{‰}$, -6.5‰ , and 0‰ and $\text{CO}_2/^3\text{He} = 1 \times 10^{13}$, 1.5×10^9 , and 1×10^{13} , respectively (after Sano & Marty, 1995). Percent of mantle contribution is shown along the mixing line between mantle and respectively limestones and sediments. SCLM from Bräuer et al. (2016) and SMX from Martelli et al. (2014) and Gennaro et al. (2017). Samples from other sites of the Republic of North Macedonia (Temovski et al., 2020) and of the nearby northern Greece region (Daskalopoulou et al., 2018) are plotted for comparison.

with lower fluxes and therefore to higher permanence time in the soil, favoring oxidation processes. The result of H_2S oxidation is the deposition and accumulation of sulfate alteration minerals in the soil (Alpers et al., 2000).

et al., 2020), comprises Triassic evaporites in its sequence. Evaporite sulfates are also found south of Peshkopi, on the Macedonian side, near Debar (Figure 1; Jančev et al., 1999). Furthermore, sulfates may be contained in small quantities in shallow water carbonates (generally dolomites) of the sedimentary sequence of the Upper Pelagonian. Although not identified, one of these sulfate-containing sequences may be present at some depth beneath Duvalo.

Due to the active tectonic structures of the area, the sulfate-bearing strata may have been put in contact with the organic-rich shales by the fault system along the eastern part of the Ohrid graben. Even without anomalous heat fluxes, the most favorable temperature conditions for TSR may be reached at depths between 3 and 4 km considering an average geothermal gradient (30°C km^{-1}). The H_2S produced rises toward the surface through the same fault system either in the gas phase or dissolved in water. During transport, H_2S could be oxidized by oxygen-charged meteoric waters, producing H_2SO_4 . The strongly acidic solutions that will form may react with the limestones of the sedimentary sequence, producing abundant CO_2 .

Sulfuric acid may also be produced by the oxidative weathering of sulfides. In the geologic succession of the study area, sulfides (mainly pyrite) are found within the phyllite formation, at the contact with the granitoid intrusions (Dumurdzanov & Ivanovski, 1978) and may contribute to the production of the CO_2 released at Duvalo. Nevertheless, oxidation of sulfide minerals cannot explain the presence of H_2S in the released gases. Metamorphic reactions producing H_2S from sulfide minerals require high temperatures ($>450^\circ\text{C}$) and/or high pressures (Tomkins, 2010) and are therefore an improbable H_2S source for this system.

5.2. Processes Affecting Gas Composition in the Soil

Sample compositions are plotted on a $\text{N}_2\text{-O}_2\text{-CO}_2$ ternary diagram (Figure 3), which shows a mixing trend between a CO_2 -dominated component (with CO_2 concentrations $>960,000 \mu\text{mol mol}^{-1}$) and an atmospheric air component. Such a trend is typical of soil gases where low CO_2 contents correspond to low flux rates of the deep-derived gases (Figure 3). The N_2 excess with respect to the atmospheric air ratio in the soil gas sample of Velgoshti may be attributed to oxygen consumption given that the N_2/Ar ratio of the same sample is nearly identical to the atmosphere. Helium, CH_4 and H_2S are almost completely related to the deep geogenic member; the highest values being found in the sample with the highest CO_2 concentration (Figure 7). In a binary plot versus CO_2 , both CH_4 and He are mostly aligned along a mixing line with atmospheric air. Small deviations from the mixing line may derive from solubility differences when the uprising gases pass through groundwater not saturated in these gases. Few samples have CH_4 well below the mixing line indicating loss by microbial or inorganic oxidation. For H_2S , only the samples with a very low air contribution approximately follow the mixing line. Samples with $\geq 50\%$ of air contribution display H_2S values at or below the detection limit ($10 \mu\text{mol mol}^{-1}$), orders of magnitude beneath the mixing line. On its transit toward the soil surface, H_2S can be lost either by dissolution in water (higher solubility with respect to CO_2) or, more importantly, by oxidation. A higher contamination of the soil gases by air is, generally, connected

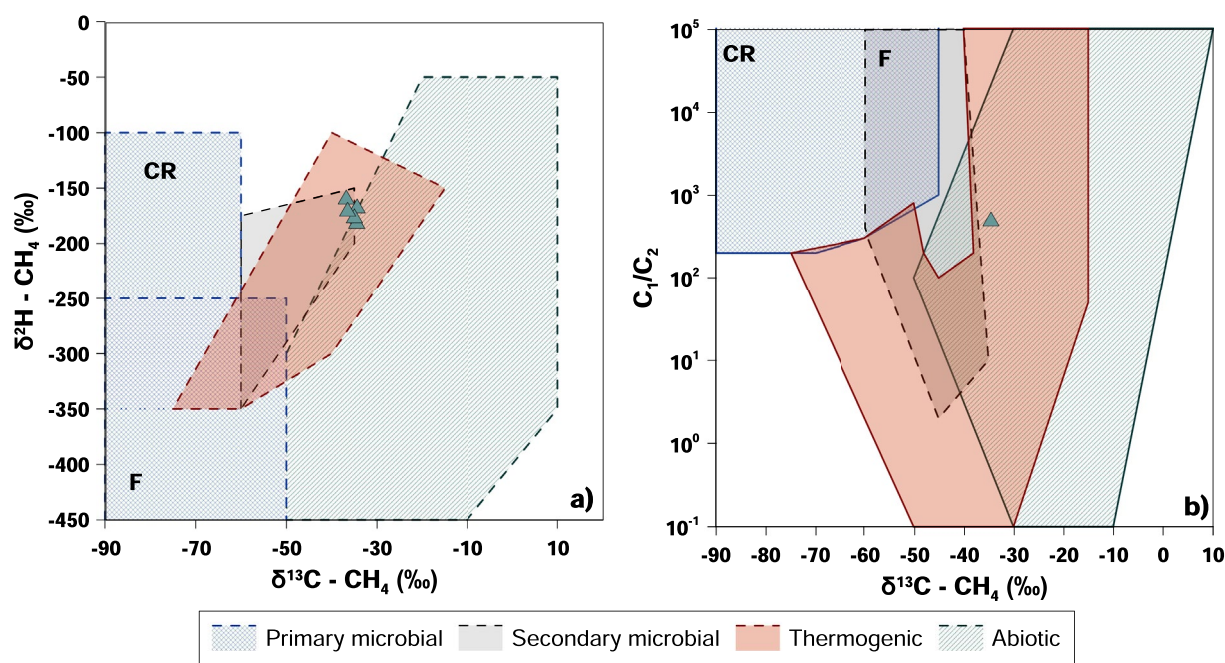


Figure 6. $\delta^{13}\text{C} - \text{CH}_4$ versus $\delta^2\text{H} - \text{CH}_4$ (a) and $\delta^{13}\text{C} - \text{CH}_4$ versus $\text{C}_1/(\text{C}_2 + \text{C}_3)$ (b) genetic diagrams (Milkov & Etiope, 2018). CR = CO₂ reduction; F = methyl-type fermentation.

Kosel 2 displays a soil gas composition close to that of atmospheric air, indicating the absence of significant deep gas exhalations. The limited alteration of the soil there may be related to the physical-chemical weathering of pyrite in the outcropping black shales (Dumurdzanov & Ivanovski, 1978). Pyrite oxidation is consistent with the low pH (~3) of the water in the small creek draining this area. Like Duvalo, the area of Kosel 2 is also crossed by some active tectonic structures (Figure 2) and we cannot exclude that it has been the site of geogenic degassing in the past. Nevertheless, the areas devoid of vegetation in this area are all very steep and are probably characterized by strong physical weathering and are not the consequence, like in Duvalo, of intense chemical alteration.

The Velgoshti sample has a higher N₂/O₂ ratio (6.1) with respect to air, which can be attributed to oxygen consumption. Although the altered soil covers a much larger area than in Kosel 2, we have no flux measurement that indicates that such alteration is linked to high gas fluxes, as in Duvalo. Our single soil gas analysis does not indicate a geogenic contribution. Nevertheless, the area deserves future study of soil CO₂ fluxes.

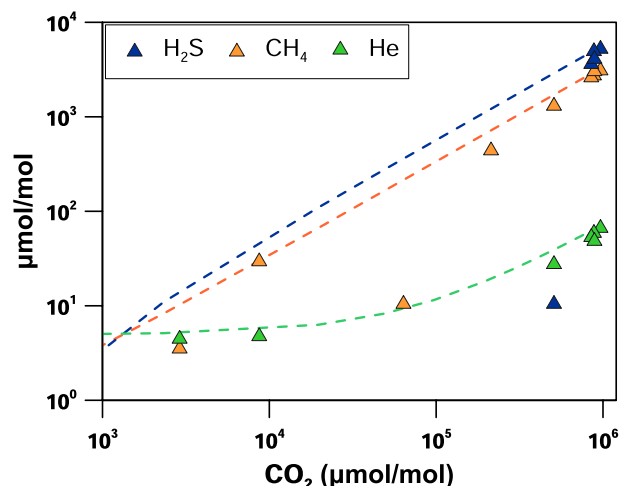


Figure 7. H₂S, CH₄, and He versus CO₂ binary plot. The dashed lines represent the mixing between atmospheric air and the deep geogenic gas.

5.3. CO₂ Flux Mapping and CO₂ Output Estimation

An estimation of CO₂ release from soil degassing has been obtained following the sGs method (Cardellini et al., 2003). The experimental variogram of the normal scores of CO₂ flux (Figure 8b) highlights two nested structures: one characterized by a shorter range (30 m) and one by a larger range (90 m), that may reflect the occurrence of a set of spatially organized small scale anomalies. The map of the CO₂ flux shows (Figure 8a) that the most anomalous degassing areas are aligned along preferential directions following the main tectonic lineament of the area. We infer that fracture-zones channel the deep gas, described also as diffuse degassing structures (Chiodini et al., 2001). Significant soil CO₂ degassing can help to detect active tectonic features as shown by Lewicki and Brantley (2000), Kämpf et al. (2013), Weinlich (2014), and Kis et al. (2017), among others. The inferred features are in concordance with

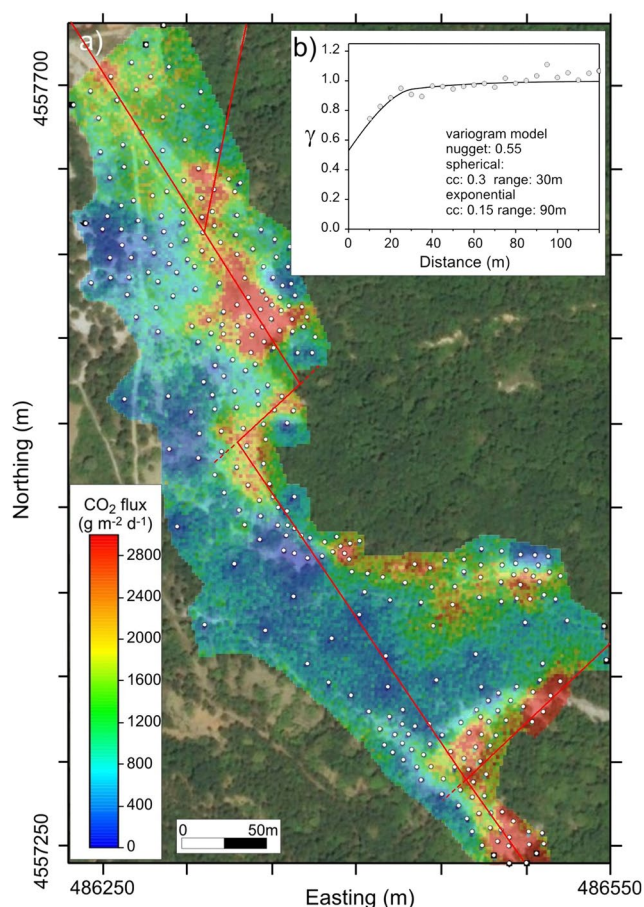


Figure 8. (a) map of the CO₂ flux; white dots refer to measured sites; red lines are inferred diffuse degassing structures which follow the directions of the tectonic lineaments defined by Dumurdzanov and Ivanovski (1978); and (b) experimental variogram and variogram model.

the lineaments showed by Dumurdzanov and Ivanovski (1978) mainly in the NNW-SSE direction but also in the NNE-SSW or NE-SW directions.

The total amount of released CO₂ estimated from the sGs results for the Duvalo site is $66.9 \pm 7.1 \text{ t d}^{-1}$ from the mapped area of $\sim 54,550 \text{ m}^2$. This CO₂ output corresponds mainly to deep CO₂, with a maximum contribution of biogenic CO₂ of 2.4 t d^{-1} assuming a biogenic CO₂ flux of $45 \text{ g m}^{-2} \text{ d}^{-1}$ (i.e., the mean CO₂ flux of population A) constant over all the area.

5.4. Duvalo in the Regional Context

The Balkan and the nearby Italian peninsulas, due to their intense geodynamic activity, are sites of widespread geogenic degassing. But, while Italy has been widely studied in the last decades (e.g., Frondini et al., 2019 and reference therein; Rogie et al., 2000; Chiodini et al., 2011), much less information is available for the Balkans. The latter is long known to be the site of countless CO₂-rich gas manifestations but relatively few have been studied to unravel the origin of the gases (Italiano et al., 2017; Marinković et al., 2012; Piperov et al., 1994; Randazzo et al., 2021; Vaselli et al., 2002). The best studied region up to now is probably Greece, the southern end of the Balkan Peninsula (Daskalopoulou et al., 2018, 2019). Even fewer studies have attempted to quantify the CO₂ output of these sites (Kis et al., 2017; Nisi et al., 2013) with the exception of those in Greece, which were recently reviewed by Daskalopoulou et al. (2019). The studied degassing systems in Greece are almost all connected to recent (Quaternary) or active volcanic activity. The output obtained here for the non-volcanic Duvalo site is comparable to the estimated CO₂ outputs of the active volcanic systems of the Aegean arc, which range from 2.6 t d^{-1} at Methana (D'Alessandro et al., 2008) to 92 t d^{-1} at Nisyros (Bini et al., 2019). Non-volcanic degassing has been detected also in Greece but until now only that of the Sperchios Basin area has been estimated, at about 27 t d^{-1} (D'Alessandro et al., 2020). The area of Florina has probably an even higher total CO₂ output, but it has not yet been quantified. Evidence of high CO₂ fluxes here comes from the extraction, by the Air Liquide Greece Company of about 80 t CO_2 per day from deep wells without apparently affecting the output of the numerous gas manifestations

of the area (Pearce et al., 2004). Furthermore, the anomalous degassing area of Florina extends beyond the border with North Macedonia into the Bitola Plain where other companies exploit the CO₂ accumulation in the subsoil (Mirčovski et al., 2015).

In Italy many non-volcanic gas manifestations are present and most have been studied, both to define the origin of the emitted gases and to quantify their CO₂ output (e.g., Chiodini et al., 1999, 2011, 2020; Frondini et al., 2008, 2012; Minissale et al., 1997; Rogie et al., 2000). Many of them have higher CO₂ outputs (e.g., Chiodini et al., 2011, 2020) with respect to Duvalo, sometimes up to more than one order of magnitude (e.g., Mefite D'Ansanto $2,000 \text{ t d}^{-1}$; Chiodini et al., 2010). But in both cases, for the Italian sites and for the Greek ones, a direct or indirect connection to the mantle is always hypothesized. In the case of Central Italy helium isotope compositions range from values around $2 R/R_A$ to about $0.02 R/R_A$. The highest $^3\text{He}/^4\text{He}$ ratios resemble the values measured in the olivine and pyroxenes of the Tuscan-Latium volcanic products (Martelli et al., 2004), linked to subduction-related carbon-rich mantle (e.g., Frezzotti et al., 2009; Martelli et al., 2004; Peccerillo, 1999), and the lower ones are interpreted as evidence for variable addition of crustal ^4He during the gas storage in crustal reservoir (e.g., Chiodini et al., 2011). Also in the case of Greece, $^3\text{He}/^4\text{He}$ up to $1.3 R/R_A$ point to substantial gas contributions from the mantle (Daskalopoulou et al., 2019).

In the case of Duvalo the contribution from the mantle seems absent or at least very low, if a MORB-type mantle end-member is assumed. A subcontinental lithospheric mantle (SCLM) type (Gautheron & Moreira, 2002) source has been hypothesized for gas manifestations in two areas at the periphery of the Balkan peninsula: Slovenia (Bräuer et al., 2016) and the South Aegean Active Volcanic Arc (Shimizu et al., 2005). Nevertheless,

these hypotheses have not been confirmed by data on fluid inclusions in mantle minerals and in the second case, they have been challenged by recent data from Kolumbo volcano whose gas emissions have He and C isotopic compositions compatible with a MORB-type mantle (Rizzo et al., 2016).

Furthermore, widespread mantle metasomatism by fluids released by the subducting slab in the central Mediterranean region has been hypothesized from isotopic composition of gas manifestations (Chiodini et al., 2011; Frondini et al., 2019; Parello et al., 2000), mantle xenoliths' fluid inclusions (Martelli et al., 2004) and petrological and geophysical data (Frezzotti et al., 2009). One of the best studied systems is the island of Stromboli where fluid inclusions in minerals of mantle xenoliths define the mantle end-member for both He (Martelli et al., 2014) and C (Gennaro et al., 2017) isotopes (Figure 5). Even stronger metasomatism has been hypothesized in the Roman Magmatic Province (central Italy) from the He isotopic composition ($0.44\text{--}1.73 R/R_A$, Martelli et al., 2004) measured in fluid inclusions trapped within olivine and pyroxene phenocrysts associated with mantle-derived basic lavas and pyroclastic rocks.

Some evidence of a metasomatized mantle beneath the southern Balkan Peninsula may come from the R/R_A values measured in gas manifestations never exceeding 1.6 in North Macedonia (Temovski et al., 2020), 1.3 in continental Greece (Daskalopoulou et al., 2018) and 0.8 in Bulgaria (Piperov et al., 1994). Furthermore, mantle metasomatism by subducting material was also invoked by Yanev et al. (2008) in their petrographic study of the Miocene to Pleistocene volcanic rocks of North Macedonia. Finally, Molnár et al. (2021), analyzing fluid inclusions in olivine phenocrysts from the Mlado Nagoričane volcanic center (North Macedonia), measured R/R_A values in the range of 3.1–4.5. These results are well below MORB or SCLM values and may also suggest a metasomatic process within the mantle below North Macedonia.

As seen from central Italy, a strongly metasomatized mantle would have He and C-isotopic values very different from a MORB-type mantle, leading to a severe underestimation of the mantle contribution in the sampled gases. However, even considering a metasomatized mantle like central Italy, the mantle contribution at Duvalo would be still low (<10%). Nevertheless, should the low or absent contribution from mantle degassing be confirmed by future studies, this would make Duvalo a very peculiar system: a relatively shallow source within the crust able to sustain fluxes of CO_2 higher than $1,000 \text{ t km}^{-2} \text{ d}^{-1}$.

6. Conclusions

The area of Ohrid is a seismically active extensional basin and the site of Duvalo corresponds to an active fault system. The Duvalo area exhibits a natural phenomenon of intense soil degassing considered as a volcanic solfatara in the local geological literature, although volcanic rocks or volcanic activity have not been found in the area. Based on the isotopic composition of the gas manifestations, we propose a tectonic origin for the phenomena. The isotope composition of helium and $\delta^{13}\text{C-CO}_2$ indicate an almost pure crustal (marine limestone) origin and mantle contribution seems absent or at most trivial (about 1%).

The presence of H_2S may be explained by thermochemical sulfate reduction (TSR), which is compatible with the isotopic composition of methane that falls within the thermogenic range. Due to the strong displacement of the tectonic structures of the area, the sulfate-bearing strata may have been put in contact with the organic-rich shales of metamorphic basement by the fault system along the eastern part of the Ohrid graben. Part of the uprising H_2S may be oxidized by oxygen-charged meteoric waters in the shallower part of the system and the sulfuric acid thus produced may react with carbonate rocks, producing abundant CO_2 with the isotopic composition measured at Duvalo.

A map of CO_2 flux shows that the most anomalous degassing areas are aligned along a NNW-SSE direction following the main tectonic lineament direction of the area. The total amount of released CO_2 for the non-volcanic Duvalo site is estimated at 66.9 t d^{-1} . The CO_2 output obtained is comparable to, albeit slightly less than the volcanic and non-volcanic systems of Greece and Italy. Nevertheless, the peculiarity of the Duvalo system lies in its ability to sustain high CO_2 fluxes ($>1,000 \text{ t km}^{-2} \text{ d}^{-1}$) with a relatively shallow crustal source.

Appendix A

The results of all CO₂ flux measurements made in the Duvalo area are reported in the following table together with the geographic coordinates of the measuring sites.

Table A1

CO₂ Flux Measurements

Point	Coordinates		CO ₂ flux (g m ⁻² d ⁻¹)	Point	Coordinates		CO ₂ flux (g m ⁻² d ⁻¹)
	<i>E</i>	<i>N</i>			<i>E</i>	<i>N</i>	
PA1	486,286	4,557,735	462	PA56	486,349	4,557,570	736
PA2	486,275	4,557,724	158	PA57	486,343	4,557,567	34,612
PA3	486,267	4,557,713	179	PA58	486,336	4,557,563	143
PA4	486,254	4,557,705	5,680	PA59	486,329	4,557,557	664
PA5	486,242	4,557,696	698	PA60	486,321	4,557,553	4,706
PA6	486,232	4,557,688	204	PA61	486,318	4,557,545	273
PA7	486,248	4,557,660	137	PA62	486,329	4,557,548	1,349
PA8	486,261	4,557,665	484	PA63	486,338	4,557,552	1,903
PA9	486,273	4,557,672	894	PA64	486,344	4,557,557	3,412
PA10	486,285	4,557,681	311	PA65	486,349	4,557,562	1,063
PA11	486,297	4,557,687	501	PA66	486,355	4,557,567	1,823
PA12	486,308	4,557,696	142	PA67	486,362	4,557,561	17,139
PA13	486,317	4,557,661	28.7	PA68	486,354	4,557,555	12,996
PA14	486,306	4,557,650	3,263	PA69	486,345	4,557,548	59,259
PA15	486,297	4,557,643	491	PA70	486,337	4,557,542	1,815
PA16	486,287	4,557,637	240	PA71	486,339	4,557,535	300
PA17	486,279	4,557,634	1,687	PA72	486,347	4,557,522	282
PA18	486,268	4,557,632	198	PA73	486,355	4,557,516	1,250
PA19	486,260	4,557,629	301	PA74	486,362	4,557,507	5,140
PA20	486,252	4,557,622	41.8	PA75	486,359	4,557,500	1.34
PA21	486,239	4,557,618	30.3	PA76	486,351	4,557,508	2,989
PA22	486,261	4,557,605	13.6	PA77	486,342	4,557,511	211
PA23	486,274	4,557,609	32.4	PA78	486,329	4,557,509	249
PA24	486,286	4,557,613	99.6	PA79	486,316	4,557,508	488
PA25	486,297	4,557,618	61.5	PA80	486,302	4,557,507	7.02
PA26	486,308	4,557,622	4,158	PA81	486,307	4,557,494	11.9
PA27	486,314	4,557,625	798	PA82	486,319	4,557,495	5,746
PA28	486,328	4,557,637	1,631	PA83	486,333	4,557,497	1,061
PA29	486,331	4,557,642	46.5	PA84	486,345	4,557,499	863
PA30	486,343	4,557,614	129	PA85	486,348	4,557,464	1,151
PA31	486,328	4,557,611	189	PA86	486,335	4,557,463	3,790
PA32	486,319	4,557,607	587	PA87	486,321	4,557,459	17.2
PA33	486,308	4,557,602	1,595	PA88	486,330	4,557,448	15.4
PA34	486,299	4,557,597	167	PA89	486,342	4,557,454	950
PA35	486,289	4,557,594	75.7	PA90	486,350	4,557,456	622
PA36	486,276	4,557,589	479	PA91	486,363	4,557,456	7.96
PA37	486,265	4,557,586	48.2	PA92	486,359	4,557,448	36.6
PA38	486,254	4,557,586	66.6	PA93	486,359	4,557,440	671

Table A1
Continued

Point	Coordinates		CO ₂ flux (g m ⁻² d ⁻¹)	Point	Coordinates		CO ₂ flux (g m ⁻² d ⁻¹)
	E	N			E	N	
PA39	486,242	4,557,583	24.3	PA94	486,363	4,557,438	204
PA40	486,264	4,557,576	60.1	PA95	486,367	4,557,433	1,401
PA41	486,282	4,557,584	393	PA96	486,372	4,557,432	120
PA42	486,293	4,557,589	100	PA97	486,381	4,557,430	2,089
PA43	486,304	4,557,593	353	PA98	486,396	4,557,429	1,981
PA44	486,314	4,557,597	833	PA99	486,390	4,557,427	1,776
PA45	486,329	4,557,600	2,592	PA100	486,393	4,557,423	4,273
PA46	486,338	4,557,603	378	PA101	486,406	4,557,411	535
PA47	486,351	4,557,609	125	PA102	486,415	4,557,409	823
PA48	486,359	4,557,592	60.5	PA103	486,428	4,557,406	398
PA49	486,350	4,557,586	4.93	PA104	486,434	4,557,417	1,688
PA50	486,344	4,557,578	864	PA105	486,443	4,557,414	1,438
PA51	486,336	4,557,574	6,401	PA106	486,452	4,557,419	476
PA52	486,329	4,557,570	6,127	PA107	486,444	4,557,403	490
PA53	486,321	4,557,566	499	PA108	486,458	4,557,403	612
PA54	486,312	4,557,561	6,409	PA109	486,473	4,557,397	407
PA55	486,302	4,557,557	975	PA110	486,473	4,557,409	1,280
PA111	486,473	4,557,416	1,074	PA167	486,445	4,557,380	678
PA112	486,474	4,557,426	34.3	PA168	486,470	4,557,363	15.3
PA113	486,494	4,557,417	95.3	PA169	486,474	4,557,344	54.1
PA114	486,497	4,557,422	4.24	PA170	486,510	4,557,358	99.7
PA115	486,505	4,557,422	2.23	PA171	486,548	4,557,360	38.2
PA116	486,513	4,557,421	12.4	PA172	486,546	4,557,380	61.2
PA117	486,514	4,557,412	3,070	PA173	486,525	4,557,383	48.9
PA118	486,507	4,557,416	141	PA174	486,499	4,557,382	19.0
PA119	486,500	4,557,413	2,659	PA175	486,447	4,557,348	19.1
PA120	486,505	4,557,409	2,821	PA176	486,418	4,557,344	4.71
PA121	486,493	4,557,410	2,423	PA177	486,417	4,557,362	18.4
PA122	486,419	4,557,326	135	PA178	486,385	4,557,373	14.2
PA123	486,414	4,557,319	616	PA179	486,346	4,557,377	8.59
PA124	486,432	4,557,307	560	PA180	486,309	4,557,381	13.8
PA125	486,439	4,557,304	959	PB1	486,289	4,557,711	418
PA126	486,444	4,557,297	1,050	PB2	486,278	4,557,705	859
PA127	486,451	4,557,290	1,023	PB3	486,269	4,557,697	592
PA128	486,461	4,557,283	646	PB4	486,258	4,557,691	136
PA129	486,468	4,557,279	607	PB5	486,247	4,557,680	474
PA130	486,472	4,557,269	5,848	PB6	486,254	4,557,645	51.3
PA131	486,479	4,557,261	1,642	PB7	486,262	4,557,651	305
PA132	486,483	4,557,253	14,025	PB8	486,275	4,557,654	745
PA133	486,489	4,557,250	4,194	PB9	486,285	4,557,661	55.0
PA134	486,500	4,557,240	249	PB10	486,298	4,557,667	421
PA135	486,506	4,557,246	2,510	PB11	486,311	4,557,675	163

Table A1
Continued

Point	Coordinates		CO ₂ flux (g m ⁻² d ⁻¹)	Point	Coordinates		CO ₂ flux (g m ⁻² d ⁻¹)
	E	N			E	N	
PA136	486,511	4,557,251	1,198	PB12	486,324	4,557,644	1,775
PA137	486,509	4,557,258	384	PB13	486,315	4,557,638	3,372
PA138	486,502	4,557,258	552	PB14	486,308	4,557,633	816
PA139	486,490	4,557,255	1,359	PB15	486,297	4,557,626	192
PA140	486,502	4,557,251	30,806	PB16	486,284	4,557,622	147
PA141	486,493	4,557,265	2,203	PB17	486,270	4,557,620	133
PA142	486,486	4,557,270	9,611	PB18	486,260	4,557,615	23.3
PA143	486,479	4,557,269	20.3	PB19	486,249	4,557,615	7.58
PA144	486,485	4,557,259	632	PB20	486,329	4,557,623	216
PA145	486,469	4,557,288	2,024	PB21	486,316	4,557,617	1,474
PA146	486,476	4,557,280	584	PB22	486,309	4,557,613	584
PA147	486,470	4,557,308	940	PB23	486,299	4,557,608	131
PA148	486,474	4,557,316	1,369	PB24	486,289	4,557,605	275
PA149	486,478	4,557,323	395	PB25	486,279	4,557,601	15.8
PA150	486,483	4,557,330	383	PB26	486,266	4,557,598	22.3
PA151	486,491	4,557,336	943	PB27	486,254	4,557,598	5.91
PA152	486,504	4,557,323	1,375	PB28	486,269	4,557,563	53.7
PA153	486,510	4,557,329	15,000	PB29	486,281	4,557,568	761
PA154	486,520	4,557,347	8,363	PB30	486,291	4,557,575	29.5
PA155	486,515	4,557,339	8,945	PB31	486,304	4,557,579	53.6
PA156	486,473	4,557,326	2,790	PB32	486,319	4,557,583	158
PA157	486,466	4,557,317	8,036	PB33	486,333	4,557,586	2,262
PA158	486,455	4,557,306	2,192	PB34	486,345	4,557,592	410
PA159	486,282	4,557,554	14.4	PB35	486,352	4,557,598	1,011
PA160	486,262	4,557,514	7.68	PB36	486,360	4,557,604	239
PA161	486,288	4,557,516	22.9	PB37	486,361	4,557,582	20.7
PA162	486,289	4,557,485	3.65	PB38	486,356	4,557,581	38.7
PA163	486,293	4,557,439	5.31	PB39	486,346	4,557,573	6,712
PA164	486,327	4,557,417	10.7	PB40	486,354	4,557,574	1,157
PA165	486,362	4,557,397	15.0	PB41	486,363	4,557,575	10.0
PA166	486,401	4,557,387	5.19	PB42	486,359	4,557,569	535
PB43	486,367	4,557,569	3,909	PB93	486,486	4,557,395	324
PB44	486,370	4,557,563	1,617	PB94	486,495	4,557,396	282
PB45	486,368	4,557,557	57.6	PB95	486,502	4,557,396	1,926
PB46	486,362	4,557,554	29.4	PB96	486,511	4,557,398	453
PB47	486,365	4,557,542	57.2	PB97	486,518	4,557,396	88.2
PB48	486,373	4,557,542	13.1	PB98	486,497	4,557,404	1,572
PB49	486,375	4,557,551	656	PB99	486,508	4,557,406	587
PB50	486,351	4,557,544	46.3	PB100	486,521	4,557,410	893
PB51	486,320	4,557,558	149	PB101	486,416	4,557,310	262
PB52	486,314	4,557,553	145	PB102	486,422	4,557,316	245
PB53	486,306	4,557,548	43.9	PB103	486,427	4,557,322	176

Table A1
Continued

Point	Coordinates		CO ₂ flux (g m ⁻² d ⁻¹)	Point	Coordinates		CO ₂ flux (g m ⁻² d ⁻¹)
	E	N			E	N	
PB54	486,316	4,557,534	3.97	PB104	486,427	4,557,331	151
PB55	486,326	4,557,537	198	PB105	486,434	4,557,321	91.1
PB56	486,334	4,557,531	67.8	PB106	486,431	4,557,316	117
PB57	486,321	4,557,528	150	PB107	486,427	4,557,311	389
PB58	486,309	4,557,524	131	PB108	486,421	4,557,305	125
PB59	486,314	4,557,517	93.1	PB109	486,443	4,557,322	14.0
PB60	486,328	4,557,519	201	PB110	486,450	4,557,316	27.1
PB61	486,341	4,557,519	107	PB111	486,443	4,557,310	207
PB62	486,346	4,557,490	1,717	PB112	486,427	4,557,301	11.4
PB63	486,335	4,557,487	737	PB113	486,435	4,557,297	293
PB64	486,319	4,557,483	40.9	PB114	486,438	4,557,289	27.8
PB65	486,306	4,557,479	8.11	PB115	486,450	4,557,281	4.11
PB66	486,345	4,557,476	437	PB116	486,460	4,557,274	25.0
PB67	486,329	4,557,474	897	PB117	486,465	4,557,266	20.8
PB68	486,316	4,557,469	764	PB118	486,468	4,557,258	64.3
PB69	486,343	4,557,445	16.5	PB119	486,474	4,557,250	221
PB70	486,333	4,557,440	2,141	PB120	486,481	4,557,244	600
PB71	486,353	4,557,450	652	PB121	486,490	4,557,240	1,692
PB72	486,342	4,557,431	10.0	PB122	486,458	4,557,297	153
PB73	486,353	4,557,440	13.7	PB123	486,463	4,557,302	883
PB74	486,358	4,557,434	2.68	PB124	486,477	4,557,292	726
PB75	486,357	4,557,425	13.2	PB125	486,466	4,557,295	2,917
PB76	486,363	4,557,423	2.36	PB126	486,473	4,557,300	898
PB77	486,371	4,557,420	1.58	PB127	486,479	4,557,309	767
PB78	486,379	4,557,421	2.36	PB128	486,482	4,557,315	565
PB79	486,386	4,557,424	1,270	PB129	486,488	4,557,324	981
PB80	486,388	4,557,433	59.7	PB130	486,499	4,557,332	685
PB81	486,395	4,557,419	1,017	PB131	486,504	4,557,341	947
PB82	486,402	4,557,430	588	PB132	486,508	4,557,348	149
PB83	486,397	4,557,412	544	PB133	486,495	4,557,344	97.5
PB84	486,404	4,557,400	31.4	PB134	486,484	4,557,340	34.1
PB85	486,419	4,557,395	57.9	PB135	486,478	4,557,336	43.7
PB86	486,438	4,557,394	77.9	PB136	486,471	4,557,330	190
PB87	486,457	4,557,393	2,284	PB137	486,462	4,557,323	15.0
PB88	486,463	4,557,419	676	PB138	486,407	4,557,329	123
PB89	486,463	4,557,412	84.5	PB139	486,396	4,557,339	50.0
PB90	486,486	4,557,424	871	PB140	486,383	4,557,347	67.4
PB91	486,486	4,557,416	575	PB141	486,371	4,557,358	125
PB92	486,485	4,557,406	306				

Note. Coordinates UTM zone 34 T. All measurements have been made on the 23rd and 24 August 2019, except at sites from PA 159 to PA 180 made on the second of March 2020. Temperature at 50 cm depth has been measured only at the following sites: PA57 (17.7°C), PA69 (18.1°C), PA117 (18.2°C), PA153 (18.5°C) and PA157 (17.2°C).

Data Availability Statement

Li Vigni, L., Cardellini, C., Temovski, M., Ionescu, A., Molnar, K., Palcsu, L., Gagliano, A. L., Cappuzzo, S., D'Alessandro, W., 2022. Location, chemical and isotopic composition of soil gases collected in Duvalo area, North Macedonia., Version 1.0. Interdisciplinary Earth Data Alliance (IEDA). <https://doi.org/10.26022/IEDA/112209>. Accessed 2022-01-11 Li Vigni, L., Cardellini, C., Temovski, M., Ionescu, A., Molnar, K., Palcsu, L., Gagliano, A. L., Cappuzzo, S., D'Alessandro, W., 2022. Location and soil CO₂ flux from Duvalo area, North Macedonia., Version 1.0. Interdisciplinary Earth Data Alliance (IEDA). <https://doi.org/10.26022/IEDA/112210>. Accessed 2022-01-11.

Acknowledgments

This research was funded by the DCO Grant no. 10881-TDB “Improving the estimation of tectonic carbon flux,” by the European Social Fund (PO FSE Sicilia 2014–2020) in the frame of the project “Metodi di controllo geochimico e geofisico dei fenomeni naturali sul campo ed in laboratorio” (CUP: G77B17000200009), by the Italian Ministero Istruzione Università e Ricerca (MIUR, under Grant PRIN2017–2017LMNLAW “Connect-4Carbon”), and was supported by the European Union and the State of Hungary, co-financed by the European Regional Development Fund in the project of GINOP-2.3.2-15-2016-00.009 “ICER.” Fieldwork was carried out under Research Permits Nos. UP1-11/1–691/2019 and UP1-11/1–1829/2019 issued by the Ministry of Environment and Physical Planning of the Republic of North Macedonia. The authors thank INGV-Palermo for supporting the analyses carried out in its laboratories and the technicians and responsables (Giorgio Capasso, Fausto Grassa, Ygor Oliveri, Andrea Rizzo, Aldo Sollami, Francesco Salerno, and Mariano Tantillo) for their analytical contribution. The authors are also indebted with Felipe Aguilera, Agnes Mazot, an anonymous reviewer and the editor Marie Edmonds for their critical comments which contributed to improve the manuscript.

References

- Alpers, C. N., Jambor, J. L., & Nordstrom, D. K. (Eds.). (2000). Sulfate minerals – Crystallography, geochemistry and environment significance. *Reviews in Mineralogy and Geochemistry*, 40, 608.
- Arsovsky, M., & Hadzievsky, D. (1970). Correlation between neotectonics and the seismicity of Macedonia. *Tectonophysics*, 9, 129–142. [https://doi.org/10.1016/0040-1951\(70\)90013-2](https://doi.org/10.1016/0040-1951(70)90013-2)
- Barnes, I., Irwin, W. P., & White, E. (1978). Global distribution of carbon-dioxide discharges and major zones of seismicity, scale 1:40,000,000 (Water Resources Investigation Report, WRI 78-39). U.S. Geological Survey.
- Bernard, B., Brooks, J. M., & Sackett, W. M. (1977). A geochemical model for characterization of hydrocarbon gas sources in marine sediments. In *Offshore Technology Conference*. OTC-2934-MS.
- Berner, R. A., & Lasaga, A. C. (1989). Modeling the geochemical carbon cycle. *Scientific American*, 260, 74–81.
- Bini, G., Chiodini, G., Cardellini, C., Vougioukalakis, G. E., & Bachmann, O. (2019). Diffuse emission of CO₂ and convective heat release at Nisyros caldera (Greece). *Journal of Volcanology and Geothermal Research*, 376, 44–53. <https://doi.org/10.1016/j.jvolgeores.2019.03.017>
- Bojadjeva, J., Sheshov, V., Edip, K., Chaneva, J., Kitanovski, T., & Ivanovski, D. (2019). GIS-based assessment of liquefaction potential for selected earthquake scenarios. In F. Silvestri & N. Moraci (Eds.), *Earthquake Geotechnical Engineering for Protection and Development of Environment and Constructions. Proceedings in Earth and Geosciences* (Vol. 4, pp. 1453–1460).
- Brantley, S. L., & Koepenick, K. W. (1995). Measured carbon dioxide emissions from Oldoinyo Lengai and the skewed distribution of passive volcanic fluxes. *Geology*, 23, 933–936. [https://doi.org/10.1130/0091-7613\(1995\)023<0933:MCDEFO>2.3.CO;2](https://doi.org/10.1130/0091-7613(1995)023<0933:MCDEFO>2.3.CO;2)
- Bräuer, K., Geissler, W. H., Kämpf, H., Niedermann, S., & Rman, N. (2016). Helium and carbon isotope signatures of gas exhalations in the westernmost part of the Pannonian Basin (SE Austria/NE Slovenia): Evidence for active lithospheric mantle degassing. *Chemical Geology*, 422, 60–70. <https://doi.org/10.1016/j.chemgeo.2015.12.016>
- Brune, S., Williams, S., & Müller, D. (2017). Potential links between continental rifting, CO₂ degassing and climate change through time. *Nature Geoscience*, 10, 941–947. <https://doi.org/10.1038/s41561-017-0003-6>
- Burchfiel, B. C., Nakov, R., Dumurdzanov, N., Papanikolaou, D., Tzankov, T., Serafimovski, T., et al. (2008). Evolution and dynamics of the Cenozoic tectonics of the South Balkan extensional system. *Geosphere*, 4, 919–938. <https://doi.org/10.1130/GES00169.1>
- Burton, M. R., Sawyer, G. M., & Granieri, D. (2013). Deep carbon emissions from volcanoes. In R. M. Hazen, A. P. Jones, & J. A. Baross (Eds.), *Carbon in Earth. Reviews in mineralogy and Geochemistry* (Vol. 75, pp. 323–354). <https://doi.org/10.2138/rmg.2013.75.11>. *Reviews in Mineralogy and Geochemistry*
- Cardellini, C., Chiodini, G., & Frondini, F. (2003). Application of stochastic simulation to CO₂ flux from soil: Mapping and quantification of gas release. *Journal of Geophysical Research*, 108, 2425. <https://doi.org/10.1029/2002JB002165>
- Cardellini, C., Chiodini, G., Frondini, F., Avino, R., Bagnato, E., Caliro, S., et al. (2017). Monitoring diffuse volcanic degassing during volcanic unrest: The case of Campi Flegrei (Italy). *Scientific Reports*, 7, 6757.
- Chiodini, G., Caliro, S., Cardellini, C., Avino, R., Granieri, D., & Schmidt, A. (2008). Carbon isotopic composition of soil CO₂ efflux, a powerful method to discriminate different sources feeding soil CO₂ degassing in volcanic-hydrothermal areas. *Earth and Planetary Science Letters*, 274, 372–379. <https://doi.org/10.1016/j.epsl.2008.07.051>
- Chiodini, G., Caliro, S., Cardellini, C., Frondini, F., Inguaggiato, S., & Matteucci, F. (2011). Geochemical evidence for and characterization of CO₂ rich gas sources in the epicentral area of the Abruzzo 2009 earthquakes. *Earth and Planetary Science Letters*, 304, 389–398. <https://doi.org/10.1016/j.epsl.2011.02.016>
- Chiodini, G., Cardellini, C., Di Luccio, F., Selva, J., Frondini, F., Caliro, S., et al. (2020). Correlation between tectonic CO₂ Earth degassing and seismicity is revealed by a 10-year record in the Apennines, Italy. *Science Advances*, 6, eabc2938. <https://doi.org/10.1126/sciadv.abc2938>
- Chiodini, G., Cioni, R., Guidi, M., Raco, B., & Marini, L. (1998). Soil CO₂ flux measurements in volcanic and geothermal areas. *Applied Geochemistry*, 13, 543–552. [https://doi.org/10.1016/S0883-2927\(97\)00076-0](https://doi.org/10.1016/S0883-2927(97)00076-0)
- Chiodini, G., Frondini, F., Kerrick, D. M., Rogie, J., Parello, F., Peruzzi, L., & Zanzari, A. R. (1999). Quantification of deep CO₂ fluxes from central Italy: Examples of carbon balance for regional aquifers and soil degassing. *Chemical Geology*, 159, 205–222. [https://doi.org/10.1016/S0009-2541\(99\)00030-3](https://doi.org/10.1016/S0009-2541(99)00030-3)
- Chiodini, G., Frondini, F., Cardellini, C., Granieri, D., Marini, L., & Ventura, G. (2001). CO₂ degassing and energy release at Solfatara volcano, Campi Flegrei, Italy. *Journal of Geophysical Research*, 106, 16213–16221. <https://doi.org/10.1029/2001JB000246>
- Chiodini, G., Frondini, F., Cardellini, C., Parello, F., & Peruzzi, L. (2000). Rate of diffuse carbon dioxide Earth degassing estimated from carbon balance of regional aquifers: The case of central Apennine, Italy. *Journal of Geophysical Research*, 105(B4), 8423–8434. <https://doi.org/10.1029/1999JB900355>
- Chiodini, G., Granieri, D., Avino, R., Caliro, S., Costa, A., Minopoli, C., & Vilardo, G. (2010). Nonvolcanic CO₂ Earth degassing: Case of Mefite d'Ansanto (southern Apennines), Italy. *Geophysical Research Letters*, 37, L11303. <https://doi.org/10.1029/2010GL042858>
- D'Alessandro, W., Brusca, L., Kyriakopoulos, K., Michas, G., & Papadakis, G. (2008). Methana, the westernmost active volcanic system of the South Aegean arc (Greece): Insight from fluids geochemistry. *Journal of Volcanology and Geothermal Research*, 178, 818–828. <https://doi.org/10.1016/j.jvolgeores.2008.09.014>
- D'Alessandro, W., Li Vigni, L., Gagliano, A. L., Calabrese, S., Kyriakopoulos, K., & Daskalopoulou, K. (2020). CO₂ release to the atmosphere from thermal springs of Sperchios Basin and northern Euboea (Greece): The contribution of “hidden” degassing. *Applied Geochemistry*, 119, 104660. <https://doi.org/10.1016/j.apgeochem.2020.104660>

- Daskalopoulou, K., Calabrese, S., Gagliano, A. L., & D'Alessandro, W. (2019). Estimation of the geogenic carbon degassing of Greece. (Greece): The contribution of "hidden" degassing. *Applied Geochemistry*, 106, 60–74. <https://doi.org/10.1016/j.apgeochem.2019.04.018>
- Daskalopoulou, K., Calabrese, S., Grassa, F., Kyriakopoulos, K., Parello, F., Tassi, F., & D'Alessandro, W. (2018). Origin of methane and light hydrocarbons in natural fluid emissions: A key study from Greece. *Chemical Geology*, 479, 286–301. <https://doi.org/10.1016/j.chemgeo.2018.01.027>
- David, M. (1977). *Geostatistical ore reserve estimation* (p. 364). Developments in Geomathematics 2. Elsevier.
- Delmelle, P., & Stix, J. (1999). Volcanic gases. In H. Sigurdsson, B. F. Houghton, S. R. McNutt, H. Rymer, & J. Stix (Eds.), *Encyclopedia of volcanoes*. Academic Press.
- Deutsch, C. V., & Journel, A. G. (1998). *Gslib: Geostatistical software library and user's guide* (2nd ed.). Oxford University Press.
- Dumurdzanov, N., & Ivanovski, T. (1978). *Map and explanatory notes of the basic geological map 1:100,000 (map sheets Ohrid and Pogradec) of the Socialist Federal Republic of Yugoslavia* (Vol. 51). Federal Geological Survey.
- Dumurdzanov, N., Milutinovic, Z., & Salis, R. (2016). Seismotectonic zones and seismic hazard in the Republic of Macedonia. In S. Lepitkova & B. Boev (Eds.), (Vol. 1, pp. 477–491). *Proceedings of the third congress of Geologists of republic of Macedonia, Geologica Macedonica, special edition 4*.
- Dumurdzanov, N., Serafimovski, T., & Burchfiel, B. C. (2005). Cenozoic tectonics of Macedonia and its relation to the South Balkan extensional regime. *Geosphere*, 1, 1–22.
- Faulkner, D. R., Jackson, C. A. L., Lunn, R. J., Schlische, R. W., Shipton, Z. K., Wibberley, C. A. J., & Withjack, M. O. (2010). A review of recent developments concerning the structure, mechanics and fluid flow properties of fault zones. *Journal of Structural Geology*, 32, 1557–1575. <https://doi.org/10.1016/j.jsg.2010.06.009>
- Fischer, T. P., & Aiuppa, A. (2020). AGU Centennial Grand Challenge: Volcanoes and deep carbon global CO₂ emissions from subaerial volcanism—Recent progress and future challenges. *Geochemistry, Geophysics, Geosystems*, 21, e2019GC008690. <https://doi.org/10.1029/2019GC008690>
- Fischer, T. P., Arellano, S., Carn, S., Aiuppa, A., Galle, B., Allard, P., et al. (2019). The emissions of CO₂ and other volatiles from the world's subaerial volcanoes. *Science Reports*, 9(1), 18716. <https://doi.org/10.1038/s41598-019-54682-41591>
- Fraser, A., Nishani, P., Bushati, S., & Hyseni, A. (1996). Relationship between tectonic zone of the Albanides, based on results of geophysical studies. In P. A. Ziegler, & F. Horwath (Eds.), *Peri-Tethys Memoir 2: Structure and Prospects of Alpine basins and Forelands* (Vol. 170, pp. 485–511). Memoir Musee Historie Naturel.
- Frezzotti, M. L., Peccerillo, A., & Panza, G. (2009). Carbonate metasomatism and CO₂ lithosphere–asthenosphere degassing beneath the Western Mediterranean: An integrated model arising from petrological and geophysical data. *Chemical Geology*, 262, 108–120. <https://doi.org/10.1016/j.chemgeo.2009.02.015>
- Frondini, F., Caliro, S., Cardellini, C., Chiodini, G., Morgantini, N., & Parello, F. (2008). Carbon dioxide degassing from Tuscany and Northern Latium (Italy). *Global and Planetary Change*, 61, 89–102. <https://doi.org/10.1016/j.gloplacha.2007.08.009>
- Frondini, F., Cardellini, C., Caliro, S., Beddini, G., Rosiello, A., & Chiodini, G. (2019). Measuring and interpreting CO₂ fluxes at regional scale: The case of the Apennines, Italy. *Journal of the Geological Society*, 176, 408–416. <https://doi.org/10.1144/jgs2017-169>
- Frondini, F., Cardellini, C., Caliro, S., Chiodini, G., & Morgantini, N. (2012). Regional groundwater flow and interactions with deep fluids in western Apennine: The case of Narni–Amelia chain (Central Italy). *Geofluids*, 12, 182–196. <https://doi.org/10.1111/j.1468-8123.2011.00356.x>
- Gautheron, C., & Moreira, M. (2002). Helium signature of the subcontinental lithospheric mantle. *Earth and Planetary Science Letters*, 199, 39–47. [https://doi.org/10.1016/S0012-821X\(02\)00563-0](https://doi.org/10.1016/S0012-821X(02)00563-0)
- Gennaro, M. E., Grassa, F., Martelli, M., Renzulli, A., & Rizzo, A. L. (2017). Carbon isotope composition of CO₂-rich inclusions in cumulate-forming mantle minerals from Stromboli volcano (Italy). *Journal of Volcanology and Geothermal Research*, 346, 95–103. <https://doi.org/10.1016/j.jvolgeores.2017.04.001>
- Hoffmann, N., Reichert, K., Fernández-Steeger, T., & Grützner, C. (2010). Evolution of ancient Lake Ohrid: A tectonic perspective. *Biogeosciences*, 7, 3377–3386.
- Hunt, J. A., Zafu, A., Mather, T. A., Pyle, D. M., & Barry, P. H. (2017). Spatially variable CO₂ degassing in the main Ethiopian rift: Implications for magma storage, volatile transport, and rift-related emissions. *Geochemistry, Geophysics, Geosystems*, 18, 3714–3737. <https://doi.org/10.1002/2017GC006975>
- Iloski, G., Ivanovski, G., & Orcheski, S. (1957). Извештај за сулфурните појави кај с.Косел-Охридско, Биро за геолошки истражувања – Охрид. Report on sulfur phenomena in the village of Kosel-Ohrid, Bureau for Geological Research – Ohrid. (in Macedonian).
- IPCC. (2014). *Climate change 2014: Synthesis report*. Contribution of Working Groups I, II and III to the Fifth Assessment Report of the Intergovernmental Panel on Climate Change. In Core Writing Team, R. K. Pachauri, & L. A. Meyer (Eds.), (p. 151). IPCC.
- Irwin, W. P., & Barnes, I. (1980). Tectonic relations of carbon dioxide discharges and earthquakes. *Journal of Geophysical Research*, 85, 3115–3121. <https://doi.org/10.1029/JB085iB06p03115>
- Italiano, F., Kis, B.-M., Baci, C., Ionescu, A., Harangi, S., & Palcsu, L. (2017). Geochemistry of dissolved gases from the Eastern Carpathians – Transylvanian basin boundary. *Chemical Geology*, 469, 117–128. <https://doi.org/10.1016/j.chemgeo.2016.12.019>
- Jančev, S., Pezdič, J., Szaran, J., & Halas, S. (1999). Characteristics of sulphate occurrences near Kosovrasti, Macedonia. *RMZ*, 46(3), 501–508.
- Kämpf, H., Bräuer, K., Schumann, J., Hahne, K., & Strauch, G. (2013). CO₂ discharge in an active, non-volcanic continental rift area (Czech Republic): Characterization ($\delta^{13}\text{C}$, $^3\text{He}/^4\text{He}$) and quantification of diffuse and vent CO₂ emissions. *Chemical Geology*, 339, 71–83. <https://doi.org/10.1016/j.chemgeo.2012.08.005>
- Kerrick, D. M. (2001). Present and past nonanthropogenic CO₂ degassing from the solid earth. *Reviews of Geophysics*, 39, 565–585. <https://doi.org/10.1029/2001RG000105>
- Kerrick, D. M., & Caldeira, K. (1993). Metamorphic CO₂ degassing from orogenic belts. *Chemical Geology*, 145, 213–232. [https://doi.org/10.1016/S0009-2541\(97\)00144-7](https://doi.org/10.1016/S0009-2541(97)00144-7)
- Kerrick, D. M., McKibben, M. A., Seward, T. M., & Caldeira, K. (1995). Convective hydrothermal CO₂ emission from high heat flow region. *Chemical Geology*, 121, 285–293. [https://doi.org/10.1016/0009-2541\(94\)00148-2](https://doi.org/10.1016/0009-2541(94)00148-2)
- King, C. Y. (1986). Gas geochemistry applied to earthquake prediction: An overview. *Journal of Geophysical Research*, 91(B12), 12269–12281. <https://doi.org/10.1029/JB091iB12p12269>
- Kis, B. M., Ionescu, A., Cardellini, C., Harangi, S., Baci, C., Caracausi, C., & Viveiros, F. (2017). Quantification of carbon dioxide emissions of Ciomadul, the youngest volcano of the Carpathian-Pannonian Region (Eastern-Central Europe, Romania). *Journal of Volcanology and Geothermal Research*, 341, 119–130. <https://doi.org/10.1016/j.jvolgeores.2017.05.025>
- Kotevski, G. (1987). *Hidrogeologija na mineralnite, termalnite i termomineralnite vodi na teritorijata na Socijalistichka Republika Makedonija (Hydrogeology of the mineral, thermal and thermomineral waters in the territory of the Socialist Republic of Macedonia)* (p. 352). Samupravna praktika. (in Macedonian).

- Le Guern, F. (1982). Les debits de CO₂ et de SO₂ volcaniques dans l'atmosphere. *Bulletin of Volcanology*, 45(3), 197–202. <https://doi.org/10.1007/BF02597730>
- Lee, V. W., & Trifunac, M. D. (2017). Seismic hazard maps in Macedonia. *Soil Dynamics and Earthquake Engineering*, 100, 504–517. <https://doi.org/10.1016/j.soildyn.2017.06.010>
- Lewicki, J., & Brantley, S. L. (2000). CO₂ degassing along the San Andreas Fault, Parkfield, California. *Geophysical Research Letters*, 27(1), 5–8. <https://doi.org/10.1029/1999GL008380>
- Lewicki, J. L., Bergfeld, D., Cardellini, C., Chiodini, G., Granieri, D., Varley, N., & Werner, C. (2005). Comparative soil CO₂ flux measurements and geostatistical estimation methods on Masaya volcano, Nicaragua. *Bulletin of Volcanology*, 68, 76–90. <https://doi.org/10.1007/s00445-005-0423-9>
- Li Vigni, L., Cardellini, C., Temovski, M., Ionescu, A., Molnar, K., Palcsu, L., et al. (2022a). Location and soil CO₂ flux from Duvalo area, North Macedonia, version 1.0. *Interdisciplinary Earth Data Alliance (IEDA)*. <https://doi.org/10.26022/IEDA/112210>
- Li Vigni, L., Cardellini, C., Temovski, M., Ionescu, A., Molnar, K., Palcsu, L., et al. (2022b). Location, chemical and isotopic composition of soil gases collected in Duvalo area, North Macedonia, version 1.0. *Interdisciplinary Earth Data Alliance (IEDA)*. <https://doi.org/10.26022/IEDA/112209>
- Lindhorst, K., Krastel, S., Reichert, K., Stipp, M., Wagner, B., & Schwenk, T. (2015). Sedimentary and tectonic evolution of Lake Ohrid (Macedonia/Albania). *Basin Research*, 27, 84–101.
- Machel, H. G. (2001). Bacterial and thermochemical sulfate reduction in diagenetic settings — Old and new insights. *Sedimentary Geology*, 140, 143–175. [https://doi.org/10.1016/S0037-0738\(00\)00176-7](https://doi.org/10.1016/S0037-0738(00)00176-7)
- Marinković, G., Papić, P., Stojković, J., & Dragišić, V. (2012). Factors contributing to the formation of carbonated mineral water systems in Serbia. *Annales Geologiques de la Peninsule Balkanique*, 73, 117–124. <https://doi.org/10.2298/GABP1273117M>
- Markoski, B., Jovanovski, M., & Peshevski, I. (2019). *Duvalo – Dry mofette, Kosel, Ohrid*. Geomap doo, Skopje. (in Macedonian with extended summary in English).
- Martelli, M., Nuccio, P. M., Stuart, F. M., Burgess, R., Ellam, R. M., & Italiano, F. (2004). Helium-strontium isotope constraints on mantle evolution beneath the Roman Comagmatic Province, Italy. *Earth and Planetary Science Letters*, 224, 295–308. <https://doi.org/10.1016/j.epsl.2004.05.025>
- Martelli, M., Rizzo, A. L., Renzulli, A., Ridolfi, F., Arienzo, I., & Rosciglione, A. (2014). Noble-gas signature of magmas from a heterogeneous mantle wedge: The case of Stromboli volcano (Aeolian Islands, Italy). *Chemical Geology*, 368, 39–53. <https://doi.org/10.1016/j.chemgeo.2014.01.003>
- Milkov, A. V., & Etiope, G. (2018). Revised genetic diagrams for natural gases based on a global dataset of >20,000 samples. *Organic Geochemistry*, 125, 109–120. <https://doi.org/10.1016/j.orggeochem.2018.09.002>
- Minissale, A., Evans, W., Magro, G., & Vaselli, O. (1997). Multiple source components in gas manifestations from north-central Italy. *Chemical Geology*, 142, 175–192. [https://doi.org/10.1016/S0009-2541\(97\)00081-8](https://doi.org/10.1016/S0009-2541(97)00081-8)
- Mirčovski, V., Boev, B., Eftremoski, Z., Šorša, A., & Dimov, D. (2015). Hydrochemical data for the ground waters in the Bitola's part of the Pelagonia Valley, Republic of Macedonia. *Geologica Macedonica*, 29(1), 15–24.
- Molnár, K., Temovski, M., & Palcsu, L. (2021). First noble gas results from fluid inclusions of the Late Miocene-Pleistocene Macedonian volcanics. *EGU General Assembly 2021*, EGU21-9440. <https://doi.org/10.5194/egusphere-egu21-9440>
- Mörner, N. K., & Etiope, G. (2002). Carbon degassing from the lithosphere. *Global and Planetary Change*, 33, 185–203. [https://doi.org/10.1016/S0921-8181\(02\)00070-X](https://doi.org/10.1016/S0921-8181(02)00070-X)
- Mougin, P., Lamoureux-Var, V., Bariteau, A., & Huc, A. Y. (2007). Thermodynamic of thermochemical sulphate reduction. *Journal of Petroleum Science and Engineering*, 58, 413–427. <https://doi.org/10.1016/j.petrol.2007.01.005>
- Muirhead, J. D., Kattenhorn, S. A., Lee, H., Mana, S., Turrin, B. D., Fischer, T. P., et al. (2016). Evolution of upper crustal faulting assisted by magmatic volatile release during early-stage continental rift development in the East African Rift. *Geosphere*, 12, 1670–1700. <https://doi.org/10.1130/GES01375.1>
- Nisi, B., Vaselli, O., Marchev, P., & Tassi, F. (2013). Diffuse CO₂ soil flux measurements at the youngest volcanic system in Bulgaria: The 12.2 Ma old Kozuh Cryptodome. *Acta Vulcanologica*, 25(1–2), 169–177.
- Ozima, M., & Podosek, F. A. (2002). *Noble gas geochemistry* (2nd ed., p. 286). Cambridge University Press.
- Parello, F., Allard, P., D'Alessandro, W., Federico, C., Jean-Baptiste, P., & Catani, O. (2000). Isotope geochemistry of Pantelleria volcanic fluids, Sicily channel rift: A mantle volatile end-member for volcanism in southern Europe. *Earth and Planetary Science Letters*, 180, 325–339. [https://doi.org/10.1016/S0012-821X\(00\)00183-7](https://doi.org/10.1016/S0012-821X(00)00183-7)
- Pearce, J. M., Czernichowski-Lauriol, I., Lombardi, S., Brune, S., Nador, A., Baker, J., et al. (2004). A review of natural CO₂ accumulations in Europe as analogues for geological sequestration. *Geological Society London Special Publication*, 233, 29–41. <https://doi.org/10.1144/GSL.SP.2004.233.01.04>
- Peccerillo, A. (1999). Multiple mantle metasomatism in central-southern Italy: Geochemical effects, timing and geodynamic implications. *Geology*, 27, 315–318. [https://doi.org/10.1130/0091-7613\(1999\)027<0315:MMICS>2.3.CO;2](https://doi.org/10.1130/0091-7613(1999)027<0315:MMICS>2.3.CO;2)
- Piperov, N. B., Kamensky, I. L., & Tolstikhin, I. N. (1994). Isotopes of the light noble gases in mineral waters in the eastern part of the Balkan peninsula, Bulgaria. *Geochimica et Cosmochimica Acta*, 58, 1889–1898. [https://doi.org/10.1016/0016-7037\(94\)90422-7](https://doi.org/10.1016/0016-7037(94)90422-7)
- Popovska-Vasilevska, S., & Armenski, S. (2016). Geothermal potential of Macedonia and its utilization. In P. Papić (Ed.), *Mineral and thermal waters of Southeastern Europe*. Springer International Publishing Switzerland. https://doi.org/10.1007/978-3-319-25379-4_8
- Randazzo, P., Caracausi, A., Aiuppa, A., Cardellini, C., Chiodini, G., D'Alessandro, W., et al. (2021). Active degassing of deeply sourced fluids in central Europe: New evidences from a geochemical study in Serbia. *Geochemistry, Geophysics, Geosystems*, 22, e2021GC010017. <https://doi.org/10.1029/2021GC010017>
- Reichert, K., Hoffmann, N., Lindhorst, K., Krastel, S., Fernandez-Steege, T., Grutzner, C., & Wiatr, T. (2011). Active basins and neotectonics: Morphotectonics of the Lake Ohrid basin (FYROM and Albania). *Zeitschrift der Deutschen Gesellschaft für Geowissenschaften*, 162, 217–234.
- Rizzo, A. L., Caracausi, A., Chavagnac, V., Nomikou, P., Polymenakou, P. N., Mandalakis, M., et al. (2016). Kolumbo submarine volcano (Greece): An active window into the Aegean subduction system. *Science Reports*, 6, 28013. <https://doi.org/10.1038/srep28013>
- Robertson, A., & Shallo, M. (2000). Mesozoic-Tertiary tectonic evolution of Albania in its regional Eastern Mediterranean context. *Tectonophysics*, 316, 197–254. [https://doi.org/10.1016/S0040-1951\(99\)00262-0](https://doi.org/10.1016/S0040-1951(99)00262-0)
- Rogie, J. D., Kerrick, D. M., Chiodini, G., & Frondini, F. (2000). Flux measurements of nonvolcanic CO₂ emissions from some vents in central Italy. *Journal of Geophysical Research*, 105, 8435–8445. <https://doi.org/10.1029/1999JB900430>

- Sano, Y., & Marty, B. (1995). Origin of carbon in fumarolic gas from island arcs. *Chemical Geology*, 119, 265–274. [https://doi.org/10.1016/0009-2541\(94\)00097-R](https://doi.org/10.1016/0009-2541(94)00097-R)
- Sano, Y., & Wakita, H. (1985). Geographical distribution of $^3\text{He}/^4\text{He}$ ratios in Japan: Implications for arc tectonics and incipient magmatism. *Journal of Geophysical Research*, 90, 8729–8741. <https://doi.org/10.1029/JB080i010p08729>
- Schmid, S. M., Fügenschuh, B., Kounov, A., Matenco, L., Nievergelt, P., Oberhänsli, R., et al. (2020). Tectonic units of the Alpine collision zone between Eastern Alps and western Turkey. *Gondwana Research*, 78, 308–374. <https://doi.org/10.1016/j.gr.2019.07.005>
- Schoell, M. (1983). *Genetic characterization of natural gases* (Vol. 67, pp. 2225–2238). American Association of Petroleum Geologists Bulletin. <https://doi.org/10.1306/03b5b4c5-16d1-11d7-8645000102c1865d>
- Šerif, A. (2001). Rudarstvo vo Makedonija vo vreme na Osmanliskoto vladееnje (mining in Macedonia during the Ottoman Rule), INI, Logos-A, Skopje. (in Macedonian).
- Seward, T. M., & Kerrick, D. M. (1996). Hydrothermal CO_2 emission from the Taupo volcanic zone, New Zealand. *Earth and Planetary Science Letters*, 139, 105–113. [https://doi.org/10.1016/0012-821X\(96\)00011-8](https://doi.org/10.1016/0012-821X(96)00011-8)
- Shimizu, A., Sumino, H., Nagao, K., Notsu, K., & Mitropoulos, P. (2005). Variation in noble gas isotopic composition of gas samples from the Aegean arc, Greece. *Journal of Volcanology and Geothermal Research*, 140, 321–339. <https://doi.org/10.1016/j.jvolgeores.2004.08.016>
- Sinclair, A. J. (1974). Selection of threshold values in geochemical data using probability graphs. *Journal of Geochemical Exploration*, 3, 129–149. [https://doi.org/10.1016/0375-6742\(74\)90030-2](https://doi.org/10.1016/0375-6742(74)90030-2)
- Tamburello, G., Pondrelli, S., Chiodini, G., & Rouwet, D. (2018). Global-scale control of extensional tectonic of CO_2 earth degassing. *Nature Communications*, 9, 4608.
- Temovski, M., D'Alessandro, W., Ionescu, A., Li Vigni, L., Molnár, K., Palcsu, L., & Cardellini, C. (2020). Preliminary geochemical characterization of gas manifestations in North Macedonia. EGU2020-2763. EGU General Assembly 2020.
- Tomkins, A. G. (2010). Windows of metamorphic sulfur liberation in the crust: Implications for gold deposit genesis. *Geochimica et Cosmochimica Acta*, 74, 3246–3259. <https://doi.org/10.1016/j.gca.2010.03.003>
- Trojanović, S. (1925). La Solfatare de Kosel. *Annales Geologiques de la Peninsule Balkanique*, 8(1), 140–146.
- Vaselli, O., Minissale, A., Tassi, F., Magro, G., Seghedi, I., Ioane, D., & Szakács, A. (2002). A geochemical traverse across the Eastern Carpathians (Romania): Constraints on the origin and evolution of the mineral water and gas discharges. *Chemical Geology*, 182, 637–654. [https://doi.org/10.1016/S0009-2541\(01\)00348-5](https://doi.org/10.1016/S0009-2541(01)00348-5)
- Viveiros, F., Cardellini, C., Ferreira, T., Caliro, S., Chiodini, G., & Silva, C. (2010). Soil CO_2 emissions at Furnas volcano, São Miguel Island, Azores archipelago: Volcano monitoring perspectives, geomorphologic studies and land use planning application. *Journal of Geophysics Research*, 115, B12208. <https://doi.org/10.1029/2010JB007555>
- Viveiros, F., Chiodini, G., Cardellini, C., Caliro, S., Zanon, V., Silva, C., et al. (2020). Deep CO_2 emitted at Furnas do Enxofre geothermal area (Terceira Island, Azores archipelago). An approach for determining CO_2 sources and total emissions using carbon isotopic data. *Journal of Volcanology and Geothermal Research*, 401, 106968. <https://doi.org/10.1016/j.jvolgeores.2020.106968>
- Wagner, B., Reichert, B., Daut, G., Wessels, M., Matzinger, A., Schwalb, A., et al. (2008). The potential of Lake Ohrid for long-term palaeoenvironmental reconstructions. *Palaeogeography Palaeoclimatology Paleocology*, 259, 341–356. <https://doi.org/10.1016/j.palaeo.2007.10.015>
- Weinlich, F. H. (2014). Carbon dioxide controlled earthquake distribution pattern in the NW Bohemian swarm earthquake region, western Eger Rift, Czech Republic—gas migration in the crystalline basement. *Geofluids*, 14, 143–159. <https://doi.org/10.1111/gfl.12058>
- Werner, C., Fischer, T. P., Aiuppa, A., Edmonds, M., Cardellini, C., Carn, S., et al. (2019). Carbon dioxide emissions from subaerial volcanic regions: Two decades in review. In: *Deep carbon past to present* (Chap. 8, pp. 188–236). : Cambridge University Press.
- WMO. (2019). *The state of greenhouse gases in the atmosphere based on global observations through 2018*. WMO Greenhouse Gas Bulletin, n° 15.
- Yanev, Y., Boev, B., Doglioni, C., Innocenti, F., Manetti, P., Pecskay, Z., et al. (2008). Late Miocene to Pleistocene potassic volcanism in the Republic of Macedonia. *Mineralogy and Petrology*, 94, 45–60. <https://doi.org/10.1007/s00710-008-0009-2>
- Yuçe, G., Fu, C. C., D'Alessandro, W., Gulbay, A. H., Lai, C. W., Bellomo, S., et al. (2017). Geochemical characteristics of soil radon and carbon dioxide within the dead Sea Fault and Karasu Fault in the Amik basin (Hatay), Turkey. *Chemical Geology*, 469, 129–146. <https://doi.org/10.1016/j.chemgeo.2017.01.003>
- Zikov, M. (1997). Temperatura na vozduhot, termički režim i klimatska podelba spored termičkiot režim vo Republika Makedonija (Air temperature, thermal regime and climatic division according to the thermal regime in Republic of Macedonia). In M. Zikov, M. Georgieva, T. Andonovski, A. Stojmilov, V. Gramatikovski, V. Bakeva, & V. Dimitrievski (Eds.), *Vlijanieto na Sredozemnoto more vrz klimata na Republika Makedonija* (pp. 39–73). Makedonska riznica.